N O T I C E

THIS DOCUMENT HAS BEEN REPRODUCED FROM MICROFICHE. ALTHOUGH IT IS RECOGNIZED THAT CERTAIN PORTIONS ARE ILLEGIBLE, IT IS BEING RELEASED IN THE INTEREST OF MAKING AVAILABLE AS MUCH INFORMATION AS POSSIBLE

NASA Technical Memorandum 78640

(NASA-TM-78640) INTERACTION OF A TWO-DIMENSIONAL STRIP BOUNDARY LAYER WITH A THREE-DIMENSIONAL TRANSONIC SWEPT-WING CODE (NASA) 35 p HC A03/MF A01 CSCL 01A

N80-17988

Unclas
G3/02 33569

INTERACTION OF A TWO-DIMENSIONAL STRIP BOUNDARY LAYER WITH A THREE-DIMENSIONAL TRANSONIC SWEPT-WING CODE

PERRY A. NEWMAN, JAMES E. CARTER, AND
RUBY M. DAVIS

MARCH 1978

RECEIVED
MAR 1980
NASA STI FACILITY
ACCESS DEPT.

National Aeronautics and
Space Administration

Langley Research Center
Hampton, Virginia 23665

INTERACTION OF A TWO-DIMENSIONAL STRIP BOUNDARY LAYER WITH A THREE-DIMENSIONAL TRANSONIC SWEPT-WING CODE

Perry A. Newman, James E. Carter, and Ruby M. Davis
Langley Research Center

SUMMARY

A 3-D inviscid transonic analysis code has been combined with a 2-D strip integral boundary-layer technique to form an approximate interaction procedure for analyzing the flow over a high-aspect-ratio wing near cruise conditions. Converged results were obtained using this procedure for an aspect ratio 10.3 supercritical wing at $M_\infty = 0.80$ and $C_L = 0.53$, in which angle-of-attack adjustments were made during the iterative procedure in order to compensate for the viscous lift loss. Comparison of these calculations with experimental data shows generally good agreement and thus demonstrates the usefulness of this approximate procedure for obtaining transonic wing-load distributions.

INTRODUCTION

The purpose of this report is to present a brief discussion of a viscous-inviscid interaction calculation procedure for 3-D transonic swept-wing flows appropriate to transport cruise design conditions which, in view of successful comparisons with experimental data, may prove to be useful until a fully 3-D procedure becomes available. This procedure was developed during April 1977 in order to quickly assess several aerodynamic aspects of the engineering design for mounting an NASA supercritical wing on an existing drone vehicle. Specifically, an estimate was needed for both the angle-of-attack setting required to produce the transonic cruise design conditions ($M_\infty = 0.8$, $C_L = 0.53$ at altitude of 14 km (46,000 ft)) and the resulting detailed (chordwise and

spanwise) load distributions on the wing. Experimental data were not available at the time when this information was needed.

Calculation of cruise design loads at transonic speeds for a swept wing with supercritical airfoil sections requires the use of a nonlinear inviscid 3-D flow solution, in which the geometric shape has been corrected to account for a viscous boundary layer. This was found to be necessary in 2-D supercritical flows (ref. 1). An interactive calculation between the inviscid and viscous solutions should be made because of the dependence of the viscous solution on the inviscid pressure distribution and, correspondingly, the dependence of the inviscid flow on the displacement body shape. This iterative process is continued until convergence is obtained. The influence of the boundary layer on aft-loaded wings is significant since a sizable lift reduction occurs even near cruise conditions where separation effects are small. Hence, if a specified lift must be maintained, then angle-of-attack adjustments must also be included in the viscous-inviscid interaction procedure. The shock waves which tend to occur at transonic conditions further complicate this interactive process.

The procedure uses an existing 3-D, inviscid, transonic, full-potential equation, swept-wing computer program (refs. 2 and 3) and an integral formulation for calculating 2-D turbulent boundary layers (ref. 4) as coded for transonic airfoil applications (refs. 1 and 5). It is recognized that the use of a 2-D boundary-layer calculation along a streamwise strip is only approximate since it does not account for sweep and taper other than through the inviscid pressure distribution. However, comparison with some experimental data (unpublished, but taken as part of a more extensive study on several supercritical wings (ref. 6)) which were obtained subsequent to the calculations is encouraging.

DISCUSSION OF METHOD

In this section a brief discussion is presented concerning the specific inviscid and viscous computational procedures which

ORIGINAL PAGE IS
OF POOR QUALITY

were used in the present calculations. The limitations and modifications of each of these procedures as applied to the present interaction calculation are also mentioned.

Inviscid Calculation

The inviscid 3-D results were obtained using the Jameson-Caughey transonic flow analysis program FLO 22 (refs. 2 and 3). Reference 3 contains details concerning the methods upon which the program is based as well as a user's guide for the program. Briefly, this program solves a finite-difference approximation to the nonconservative form of the full potential-flow equation which has been transformed to a boundary conforming coordinate system. A conformal square-root mapping and simple numerical shearing transformation are used in each spanwise plane which allows most of the transformation derivatives to be calculated analytically and therefore results in an efficient computer code. The trailing vortex sheet is assumed to lie in a surface which leaves the trailing edge of the wing smoothly and it is not allowed to roll up nor dissipate. The basic Murman-Cole (ref. 7) technique of type-dependent operators incorporates Jameson's (ref. 8) "locally rotated" finite difference forms and convergent relaxation scheme (based on his artificial time-like analogy) in order to produce a reliable numerical solution algorithm. These solutions are obtained on a rather fine 3-D computational grid, almost 150 thousand points (192X24X32), by using external disk storage and buffering information into high-speed core only as needed.

The potential formulation is, of course, isentropic so that the results should not be expected to be a good approximation when strong shock waves occur in the solution. Furthermore, the nonconservative form of the governing equation does not produce solutions which maintain conservation of mass when shocks appear. Neither of these two limitations should prove too severe near cruise design conditions, in which case the shock waves tend to

be weak. Approximations in treating the wing tip and vortex sheet would be less accurate for wings of small aspect ratio. Recent experiences with inviscid solutions for highly tapered wings show a rather severe loss of accuracy, perhaps due to either the spanwise decrease in number of computational grid points on the wing or the increased nonorthogonality due to the high leading-edge sweep or both. In any case, for high-aspect-ratio transport-type wings near cruise design conditions, neither of these latter two limitations should be too severe.

Viscous Calculation

The boundary-layer program NASHMAC was built around a subroutine which was extracted from an existing 2-D airfoil code. It is based upon the Nash-Macdonald method (ref. 4) for calculating a 2-D turbulent boundary layer. This subroutine was taken from the Carlson program TRANDES (ref. 5); it is a derivative of the boundary-layer code found in reference 1 and is thus very similar to it. Modifications and additions were made in order to compute the displacement thickness distributions along streamwise strips at a number of spanwise locations on both surfaces of a wing. At each spanwise location, the boundary layer is computed along the local streamwise grid where the inviscid analysis code gives output pressure data. Transition from laminar to turbulent flow was assumed to occur at a specified trip line which, in the present calculations, was the same for both the upper and lower surface. The turbulent boundary-layer calculation is started slightly in front of the trip line to approximately account for the laminar boundary-layer thickness.

The same two-dimensional empiricisms were used in the present calculations as those used in reference 1 for the separation criterion and monotonicity conditions and smoothing procedure on the displacement thickness distribution. Also, as in reference 1, the trailing-edge displacement thickness is extrapolated from the upstream values and no viscous wake calculation is included.

ORIGINAL PAGE IS
OF POOR QUALITY

Interaction Procedure

Figure 1 is a simplified flow chart which depicts the major steps in the inviscid/viscous interaction. As already indicated, it was required that the present interaction procedure include a provision for obtaining the solution with a prescribed total lift for the given wing. Thus, angle-of-attack adjustments were needed in the course of the interaction since the 3-D inviscid analysis program FLO 22 does not include an option to specify C_L as an input.

The calculation is started with the given wing geometric shape and incidence which produces the prescribed total lift. Note that initially it might be necessary to iterate several times in FLO 22 in order to deduce the value of α for producing the given C_L. When one has allowed the FLO 22 solution to converge so that the C_L changes are small between each relaxation iteration, then a value of $\frac{\Delta C_L}{\Delta \alpha}$ obtained from successive solutions at somewhat different incidence can be used in linear interpolation (or nearby extrapolation) to predict a value of α required to produce the given C_L. Some computing time can be saved, however, if one has an experimentally determined value for $dC_L/d\alpha$ (perhaps from a similar wing) near the given C_L condition. Values derived both ways were used in the present calculations to estimate the next value of incidence, α, in the iteration procedure.

For a spanwise fine grid containing 32 points, FLO 22 puts 21 computational planes on the wing semispan. These are at the root station and every 5% semispan location including the tip station at 100% for the present results. (Subsequent cases have been run with the wing tip centered between computational grid planes in which case the output occurs at something less than every 5% semispan). However, the input data to program FLO 22 is limited by dimension statements (which could be easily changed) to 11 stations so that, in the present program, the upper and

lower surface boundary-layer displacement thickness distributions were computed with NASHMAC at these 11 streamwise strips along the span. As is usually found in interaction calculations, under-relaxation of the displacement thickness was required to prevent oscillations between successive iterations.

Due to time limitations, it was not possible to combine this interactive procedure into one computer program and build in an automatic convergence criterion. Rather, the 3-D inviscid program FLO 22 was run until it converged after each new displacement and angle of attack were prescribed. The magnetic tape restart capability in FLO 22 was used to store the entire solution so as to provide a good initial inviscid solution for the next interaction cycle.

Convergence of the interaction process was determined by comparing surface pressure distributions and displacement thickness distributions for the two successive interaction cycles. Since FLO 22 requires considerable computer resources, the total computer time would be reduced substantially by correcting α and updating the δ^* after 20 or so relaxation cycles in FLO 22 as is currently done in most 2-D interaction codes.

COMPARISON OF RESULTS

Comparison of several calculated and experimental results will be made and discussed in this section. All of the calculations were made for a wing alone (no fuselage) before any experimental results had been obtained. First, a brief discussion is presented for the interaction calculations along with comparisons between the inviscid results and those obtained with a viscous correction. Then comparisons are given with experimental results for a wing mounted on a fuselage.

Calculated Inviscid/Viscous Comparisons

A planform view of the wing used in the calculations is shown in figure 2. The assumed trip-line location is denoted by the

spanwise dashed line on the forward part of the wing planform which, as mentioned previously, was the same for both upper and lower wing surfaces. This wing is to be high-mounted on a drone vehicle and is about one-fifth the size of a full-scale transport wing. It has a semispan of 289.3 cm (113.9 inches) with root and tip chords of 112.3 and 32.0 cm (44.2 and 12.6 inches), respectively. The break in the trailing edge occurs at 42.6% semispan and the airfoil thickness varies from 14.9% chord at the root, through 12% chord at the break, to 10.6% chord at the tip. The sweep of the quarter-chord line of the trapezoidal planform is 27^{o} and the aspect ratio is 10.3. The design cruise conditions of $M_{\infty} = 0.80$, $C_L = 0.53$, and an altitude of 14 km (46,000 feet) result in a Reynolds number of 2.3×10^6 based on the mean aerodynamic chord of 59.7 cm (23.5 inches).

The first calculation in FLO 22 was for the geometric wing shape at zero incidence; this produced a wing lift coefficient (based on total planform area) of $C_L = 0.525$. This was deemed close enough to the prescribed design cruise value of $C_L = 0.53$ so the interaction was started; these results are denoted as "inviscid" in what follows. About 11 runs of the Jameson-Caughey FLO 22 program were made in the process of adding nine boundary-layer corrections and four angle-of-attack adjustments in order to arrive at the design cruise condition lift. It should be noted, however, that some of these runs, which were made in the early interaction cycles, were unnecessary and only served to develop the procedure shown in figure 1. Subsequent examples have been run with a few less boundary-layer interactions and much less computing time due to better use of the tape restart capability in FLO 22.

Figure 3 gives the calculated chordwise distribution of wing surface pressure coefficients, C_p, at 11 equally spaced spanwise stations along the wing. These are the 11 stations where the "effective inviscid" wing shape is redefined at each interaction for the present results. At each station, the interacted result, which is denoted as "viscous" but includes both viscous corrections

and angle-of-attack adjustments, is plotted above the inviscid one. It can be seen that the principle effect of the viscous interaction is to remove some of the aft camber in the wing. The resulting lift loss is compensated for by an increased angle of incidence, so that the prescribed design lift is achieved. The interacted calculation gives $C_L = 0.534$ for an $\alpha = 1.1^{\circ}$. Visual changes in the plotted section pressure coefficients were barely discernable in the last several interactions, thus indicating that the present calculation had converged when the calculations were terminated. The value of C_L obtained in the final four interactions (after the last angle-of-attack adjustment) were, respectively, 0.529, 0.536, 0.532, and 0.534. Large pressure changes, primarily due to shock-wave movement, occurred in the early stages of the interaction.

Plots of the streamwise boundary-layer displacement thickness (δ^*), nondimensionalized by the product of the local chord and cosine of the local slope angle, are shown in figure 4 at 11 spanwise locations where the "effective inviscid" shape was defined for FLO 22. Three curves are given for both the lower and upper wing surfaces. The curve denoted by an X is what was used with the geometric shape to obtain the viscous pressure distributions given in figure 3 (i.e., the "old" δ^*). The curve denoted by a + is the displacement thickness distributions calculated using the viscous pressure distributions given in figure 3 (i.e., the "predicted" δ^*). The solid line gives the relaxed correction which would be used to obtain the input shape for the next 3-D inviscid calculation in FLO 22 (i.e., the "new" δ^*). A relaxation factor of 0.25 was used at this stage of the interaction. The interaction calculation is converged when these three curves collapse to a single one, which, as can be seen in figure 4, was obtained at all stations on the lower wing surface and all but three on the upper surface. These three upper surface stations are at the root and tip, which were definitely the most sensitive regions in this procedure. Even at these three stations, these

slight differences in the displacement thickness did not alter the load distribution and, hence, the interaction was terminated.

Experimental/Numerical Comparisons

This wing has been tested on several different bodies for a number of conditions. To date, the experiment which most closely matches the conditions of the calculation with respect to Reynolds number based on mean wing chord, trip-line location, lift match on the wing and Mach number shift to approximately account for the presence of the fuselage was that done by Bartlett in the NASA Langley 8-Foot Transonic Pressure Wind Tunnel. The experimental data shown here have not been published but were taken as part of a more extensive study by Bartlett (ref. 6). A planform view of the wing-fuselage tested is shown in figure 5. The trip-line location is shown as a dashed line and does not correspond to what was used for most of the study in reference 6. However, additional experiments were made in which it was set to coincide with what had been used in the calculation.

Bartlett's data show that the transonic flow on this aft-loaded supercritical wing was rather sensitive to Mach number and lift changes. The influence of a finite length fuselage such as that shown in figure 5 produces not only a spanwise distribution of upwash at the leading edge of the wing but also rather appreciable chordwise and spanwise variations in Mach number. Henne and Hicks (ref. 9) used a subsonic program to determine an average Mach number shift at the wing position due to the area distribution of the fuselage; this shift is then applied to the input Mach number for the transonic wing calculation. In a similar manner, for the body of revolution equivalent to the fuselage shown in figure 5, Keller used his transonic axisymmetric code (refs. 10 and 11) and obtained an average Mach number shift of +0.007 when the forebody, cylinder, boattail, and sting shapes were included. Thus, on the basis of this estimate of the fuselage effects, it

ORIGINAL PAGE IS
OF POOR QUALITY

was determined that the earlier calculation at $M_\infty = 0.80$ should be compared with Bartlett's wing fuselage data at about $M_\infty = 0.793$.

Figure 6 is a plot of the spanwise distribution of the section normal force coefficient for both the inviscid and viscous calculations as well as the particular experimental condition which most closely fits the conditions of the calculation. The trip lines are the same and the Reynolds numbers based on the mean aerodynamic chord are 2.3×10^6 for the calculation and 2.4×10^6 in the experiment. The difference in Mach number of 0.01 is very close to the estimated 0.007 shift obtained independently from the axisymmetric transonic calculation. This figure shows then the extent to which the lift on the wing of the experimental wing-fuselage model matches that on the outboard sections of the wing-alone calculations. It is felt that this type of matching is more appropriate than matching either the total lift, C_L, or angle-of-attack, α, since the fuselage has not been modeled. It is also seen from figure 6 that the calculated spanwise load is shifted inboard when the viscous correction is included. Both, however, still show more load at the tip than the experiment. In these calculations, a computational grid plane was placed right at the wing tip; in subsequent calculations, the tip has been located between computational grid planes and the resulting load at the tip is in better agreement with experiment. The experimental values of C_n are obtained by integrating the chordwise C_p distributions at the five spanwise locations where data were taken.

Comparison of experimental and calculated surface pressure coefficients is shown in figure 7 at five spanwise locations. It can be seen that the interaction calculation results compare more favorably with the experimental results than the inviscid ones. The influence of the boundary layer is seen to be a decambering of the airfoil sections which, in the present calculation, has been compensated for by increasing the angle of attack to yield a desired lift. The agreement between the calculations and experiment at the furthermost inboard station is somewhat less

than that obtained in other regions of the wing. This is not surprising though since the body produces an increased upwash at the leading edge of the wing which, of course, is not accounted for in the wing-alone calculation.

Recall that the calculated viscous results were obtained by integrating along streamwise strips over the wing. Figure 8 shows oil flow photographs on both the upper and lower wing surface at very close to the same flow conditions for which the pressures were taken. The flow over most of the upper wing surface appears to be in the streamwise direction, but on the lower wing surface a noticeable outflow seems to be established at about 2/3 chord. This outflow is in the cove region of the supercritical section and is typical of wings which use such airfoils. Thus, the assumed streamwise run of the boundary layer probably does not give enough thickness toward the wing trailing edge on the lower surface; and, thus, the viscous interaction is underestimated in this region. This deficit can be seen at all spanwise stations in the pressure comparisons on figure 7.

CONCLUDING REMARKS

An approximate viscous-inviscid interaction procedure for analyzing 3-D swept wings at transonic cruise conditions for transports has been developed. This procedure included a means of accounting for the viscous lift loss by adjusting the angle of attack so as to maintain a prescribed lift. A converged solution was obtained for a high-aspect-ratio NASA supercritical wing which is to be used on a drone vehicle. These calculations indicate the importance of accounting for boundary-layer displacement effects on the inviscid flow for wings of this type. Comparisons of this calculation with experimental data, which were obtained after the calculations were made, shows generally good agreement except near the wing root and tip where the assumptions of the present calculation are the weakest. This good agreement indicates the usefulness of the present interaction procedure for obtaining the load

ORIGINAL PAGE IS
OF POOR QUALITY

distribution on a wing where the 3-D viscous effects are not significant. In addition, the use of a 2-D strip boundary-layer technique requires considerably less computer resources than a full 3-D boundary-layer analysis.

REFERENCES

1. Bauer, F.; Garabedian, P.; Korn, D.; and Jameson, A.: Supercritical Wing Sections II: Springer-Verlag, New York, 1975.

2. Jameson, Antony; Caughey, D. A.; Newman, P. A.; and Davis, R. M.: A Brief Description of the Jameson-Caughey NYU Transonic Swept-Wing Computer Program FLO-22. NASA TMX-73996, 1976.

3. Jameson, Antony; and Caughey, D. A.: Numerical Calculation of the Transonic Flow Past a Swept-Wing: ERDA Research and Development Report COO-3077-140, 1977.

4. Nash, J. F.; and Macdonald, A. G. J.: The Calculation of Momentum Thickness in a Turbulent Boundary Layer at Mach Numbers Up to Unity. Aero. Res. Council C.P. No. 963, 1967.

5. Carlson, Leland A.: TRANDES: A Fortran Program for Transonic Airfoil Analysis or Design. NASA CR-2821, 1977.

6. Bartlett, D. W.: Wind Tunnel Investigation of Several High Aspect-Ratio Supercritical Wing Configurations on a Wide-Body-Type Fuselage. NASA TMX-71996, 1977.

7. Murman, E. M.; and Cole, J. D.: Calculation of Plane, Steady Transonic Flows. AIAA J., vol. 9, no. 1, Jan. 1971, pp. 114-121.

8. Jameson, Antony: Iterative Solution of Transonic Flows Over Airfoils and Wings, Including Flows at Mach 1. Comm. Pure Appl. Math., vol. 27, 1974, pp. 283-309.

9. Henne, P. A.; and Hicks, R. M.: Wing Analysis Using a Transonic Potential Flow Computational Method. NASA TM 78464, 1978.

10. South, J. C., Jr.; and Jameson, Antony: Relaxation Solutions for Inviscid Axisymmetric Transonic Flow Over Blunt or Pointed Bodies. Proc. AIAA Comp. Fld. Dyns. Conf., Palm Springs, Calif., July 1973, pp. 8-17.

11. Keller, J. D.; and South, J. C., Jr.: RAXBOD: A FORTRAN Program for Inviscid Transonic Flow Over Axisymmetric Bodies. NASA TMX-72831, 1976.

ORIGINAL PAGE IS
OF POOR QUALITY

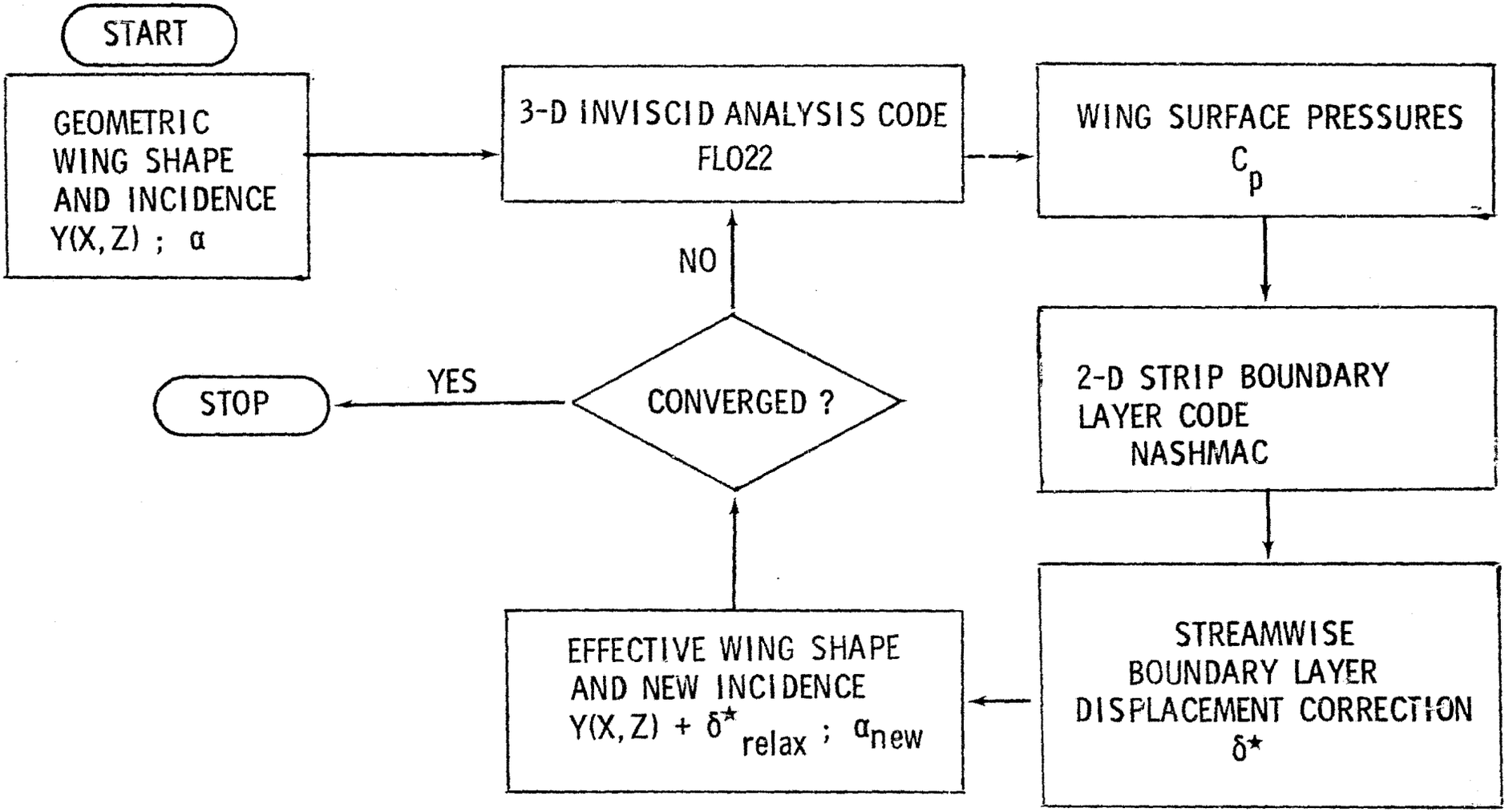

Figure 1.- Flow chart for viscous-inviscid interaction calculation procedure for 3-D transonic flow at constant lift.

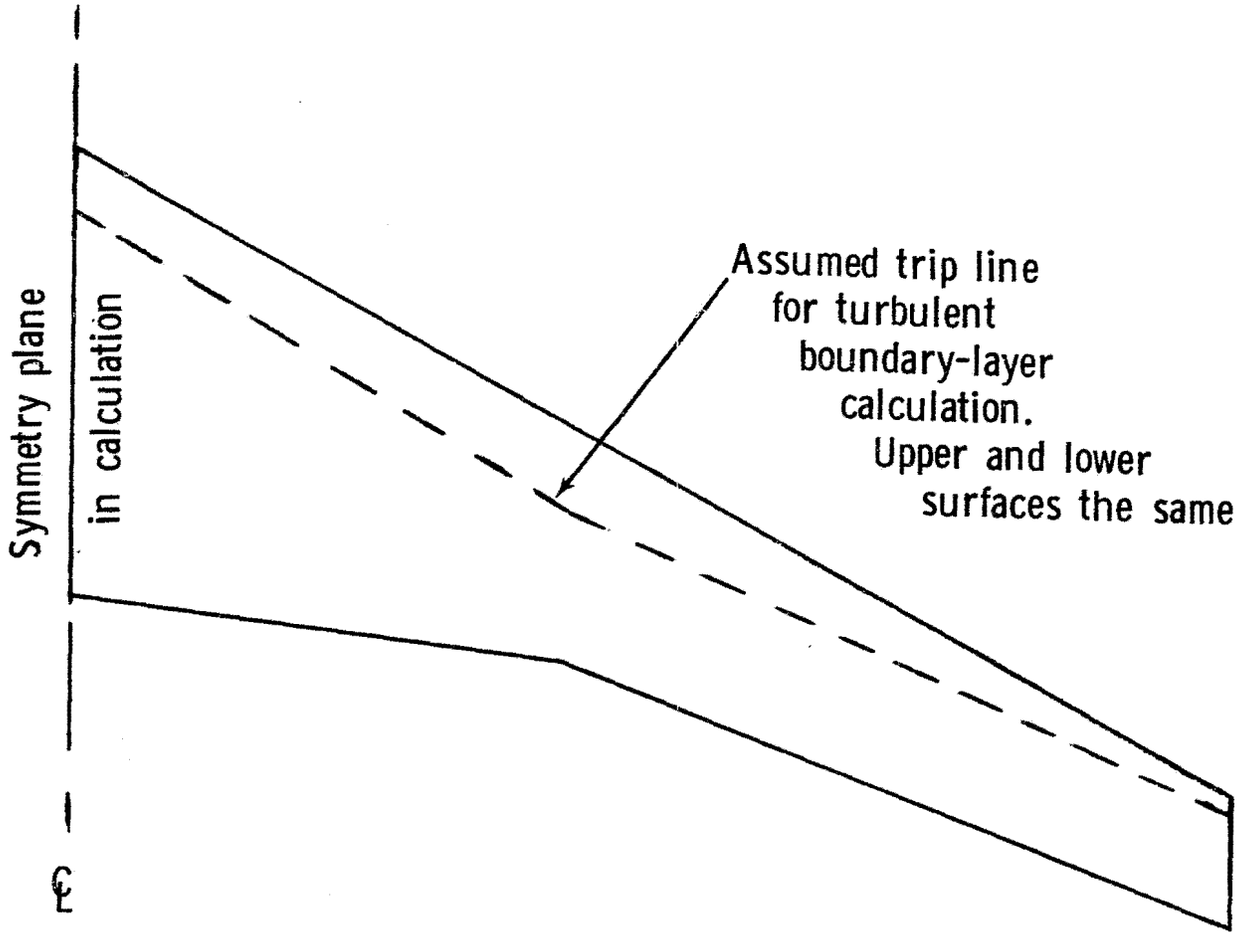

ORIGINAL PAGE IS
OF POOR QUALITY

Figure 2.- Planform view of NASA supercritical wing used in the calculations; AR = 10.3, $\Lambda_{c/4} = 27^{o}$.

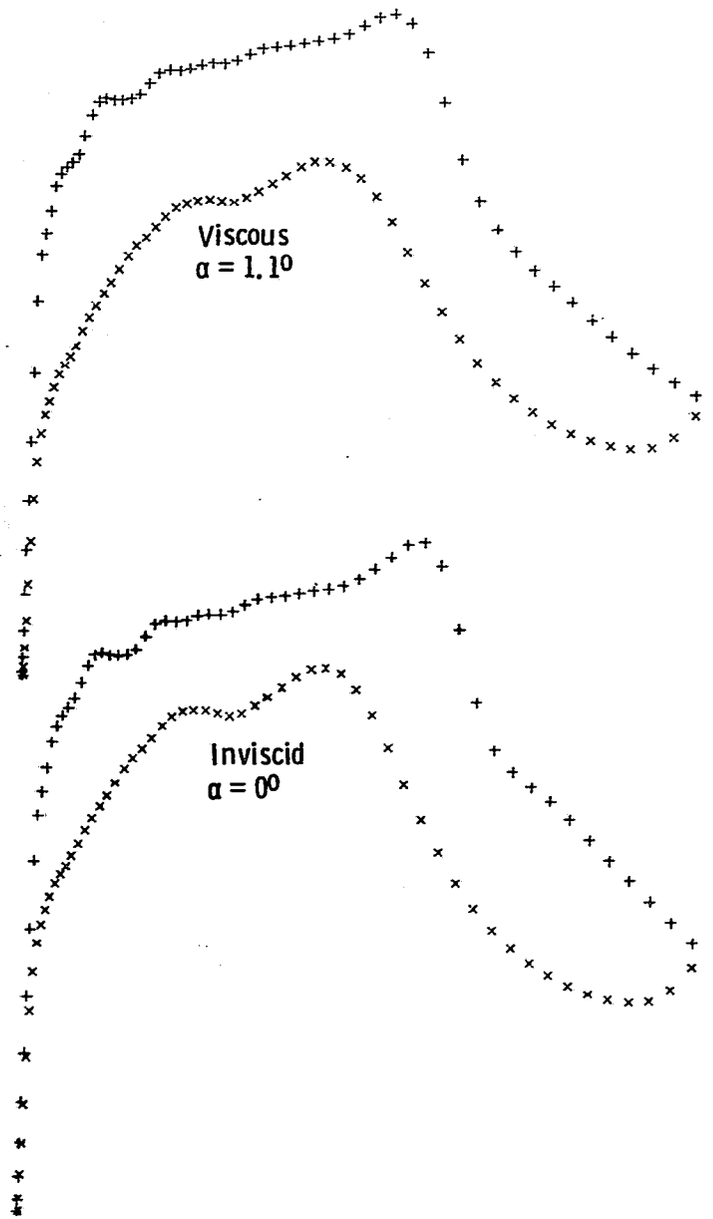

(a) 0% semispan

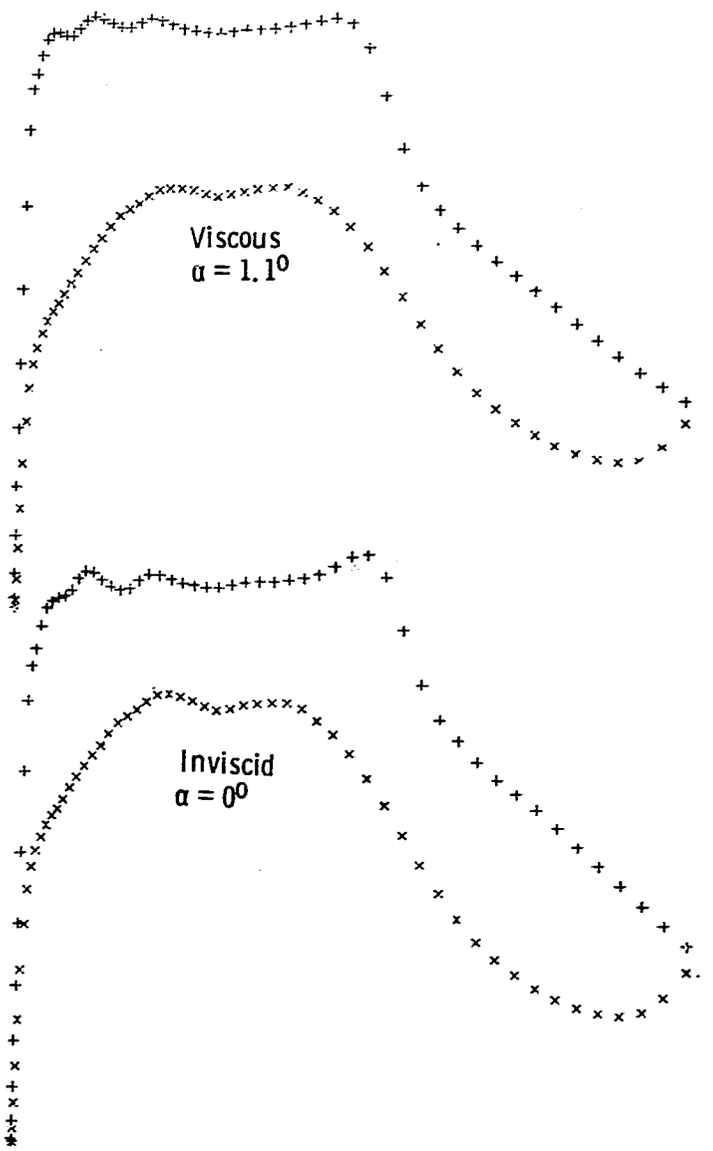

(b) 10% semispan

Figure 3.- Comparison of calculated inviscid and viscous chordwise distributions of surface pressure coefficients for a NASA Supercritical wing; $M_\infty = 0.80$, $C_L = 0.53$.

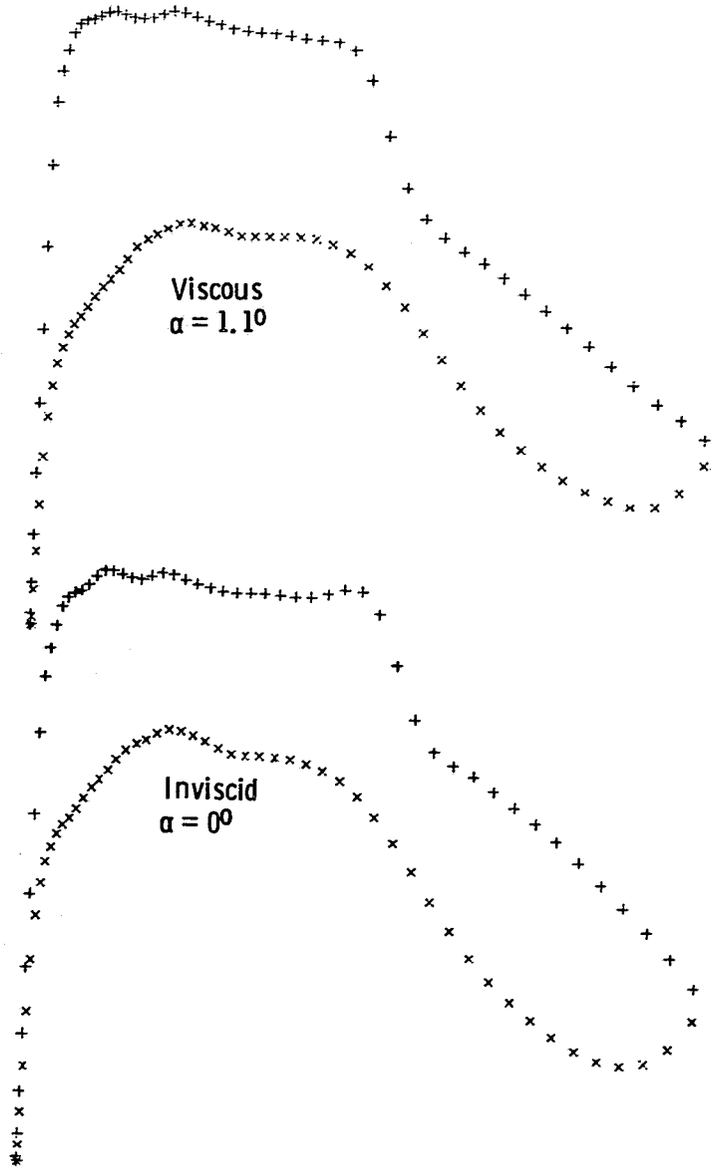

(c) 20 % semispan

ORIGINAL PAGE IS
OF POOR QUALITY

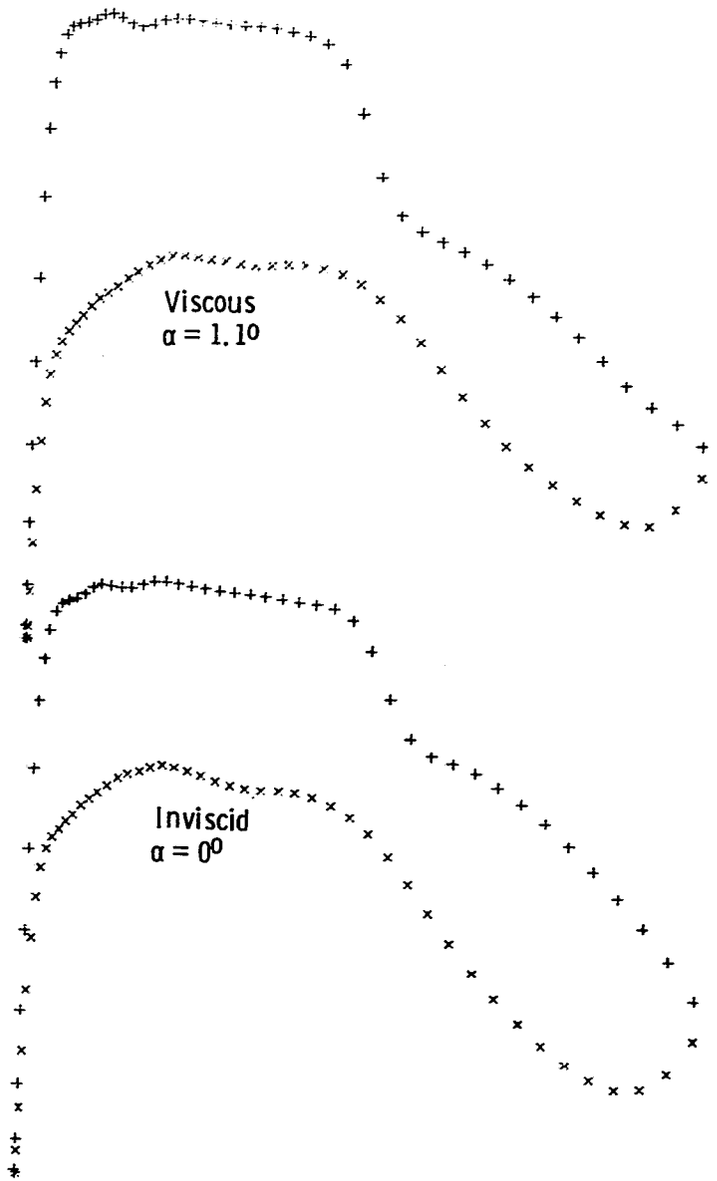

(d) 30 % semispan

Figure 3.- Continued.

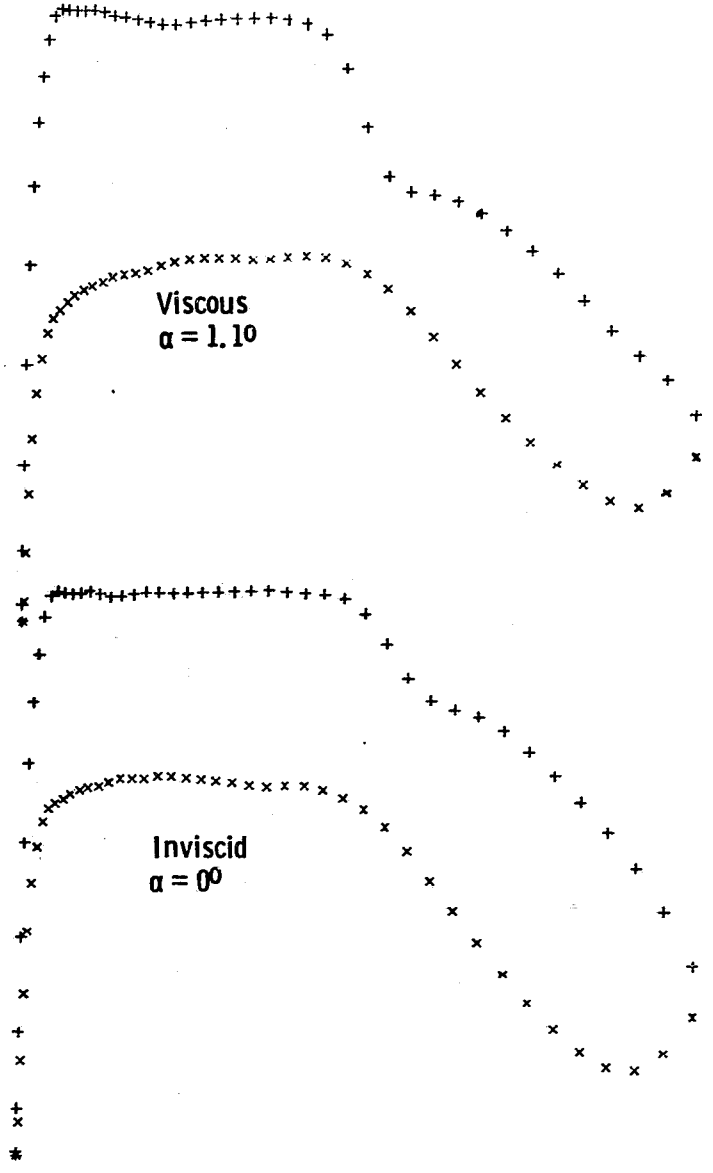

(e) 40% semispan

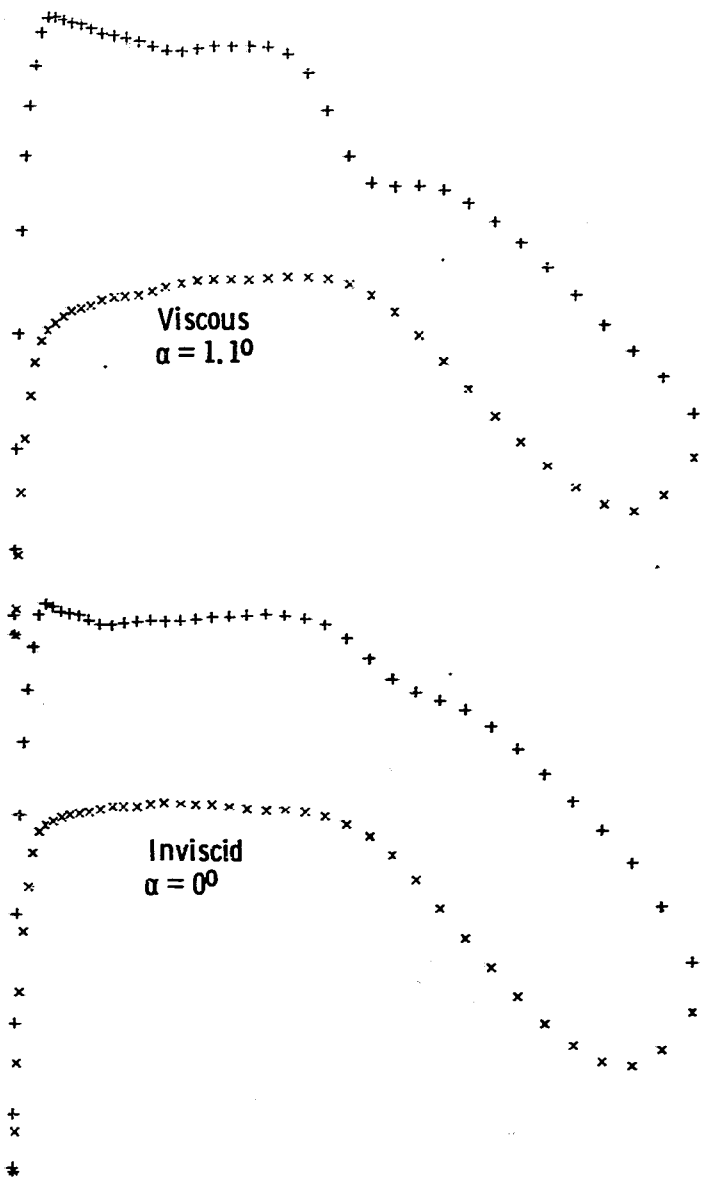

(f) 50% semispan

Figure 3.- Continued.

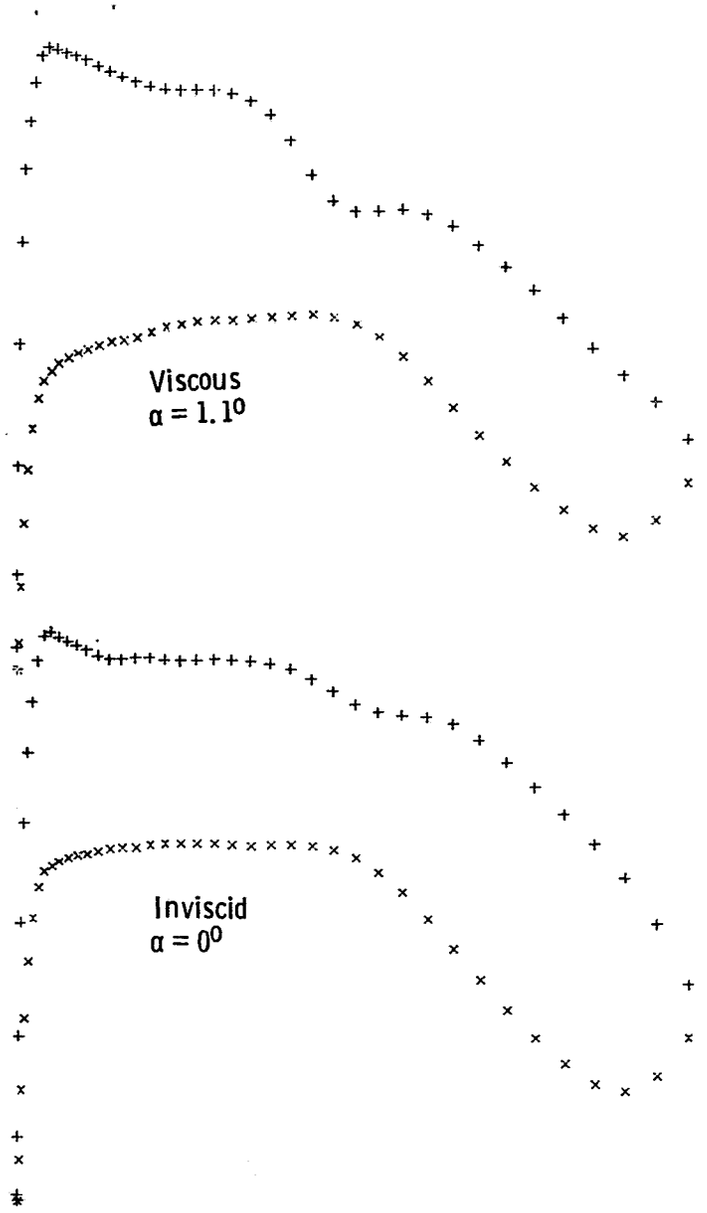

(g) 60 % semispan

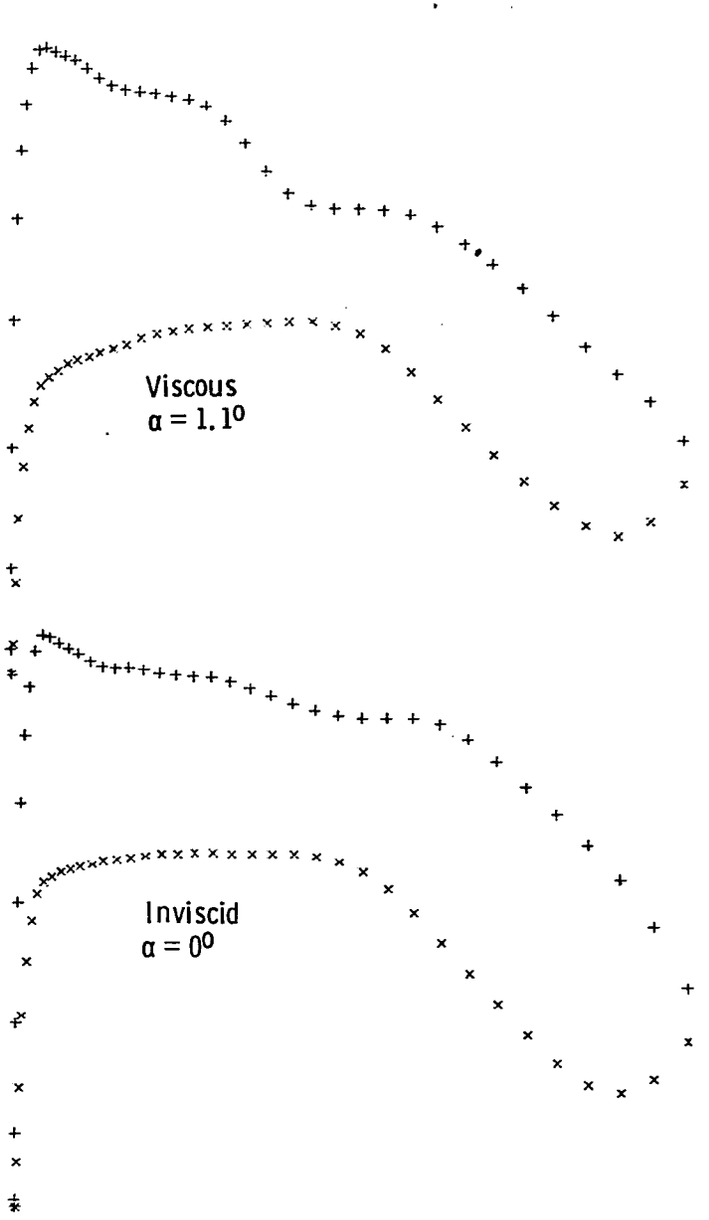

(h) 70 % semispan

Figure 3.- Continued.

Figure 3.- Continued.

ORIGINAL PAGE IS
OF POOR QUALITY

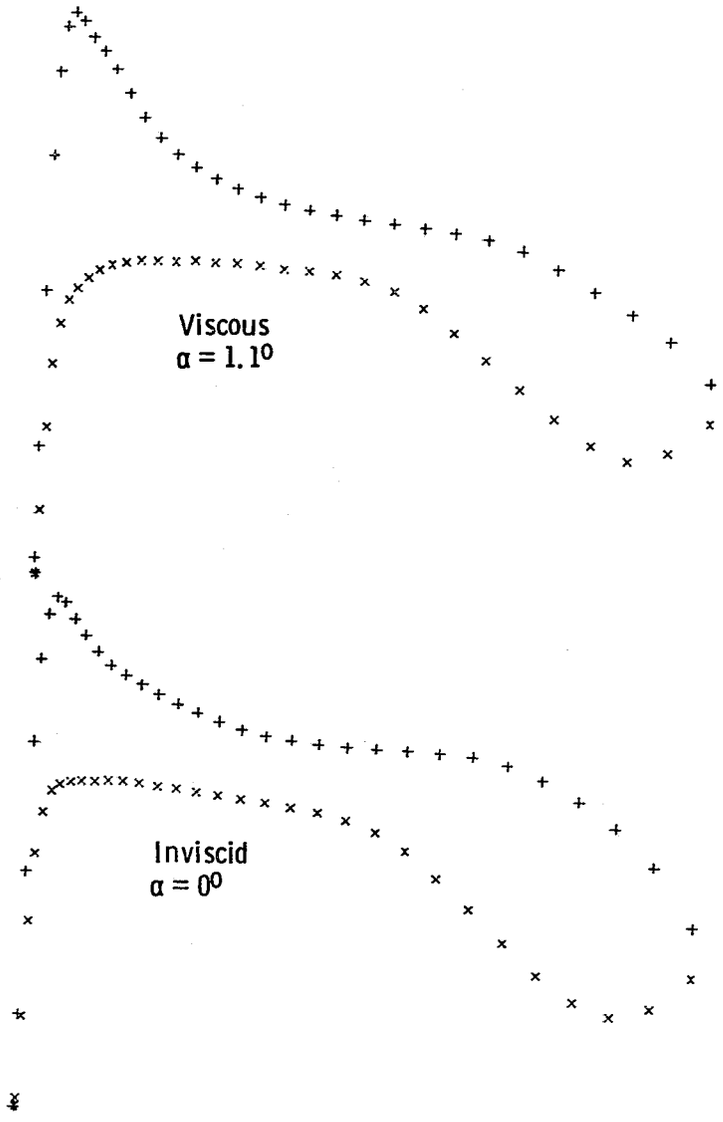

(k) 100 % semispan

Figure 3.- Concluded.

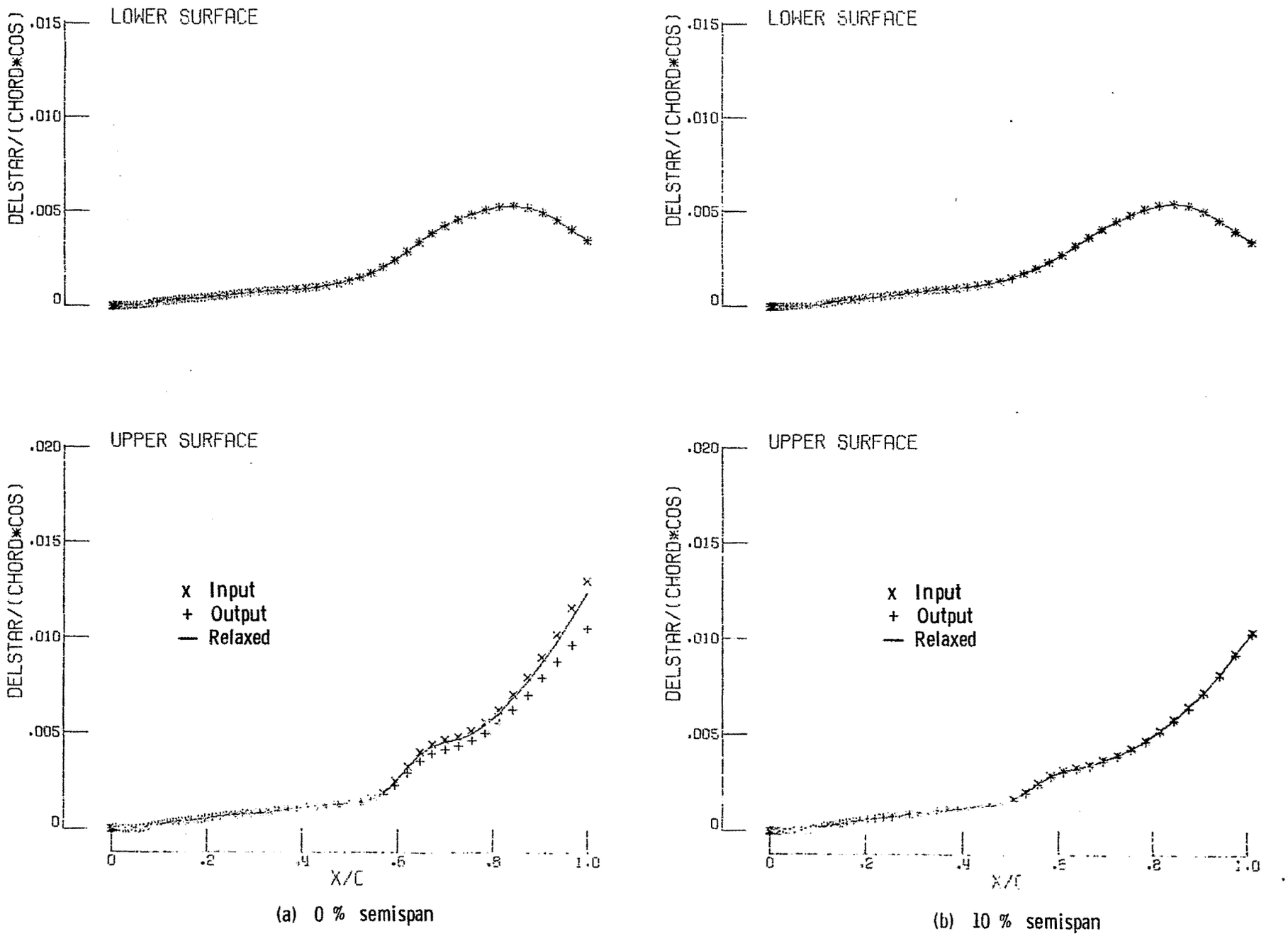

(a) 0 % semispan

(b) 10 % semispan

Figure 4.- Calculated chordwise distributions (at final interaction) of boundary layer displacement thickness for a NASA Supercritical wing; $M_\infty = 0.80$, $C_L = 0.53$, $N_{Re} = 2.3 \times 10^6$ (based on MAC).

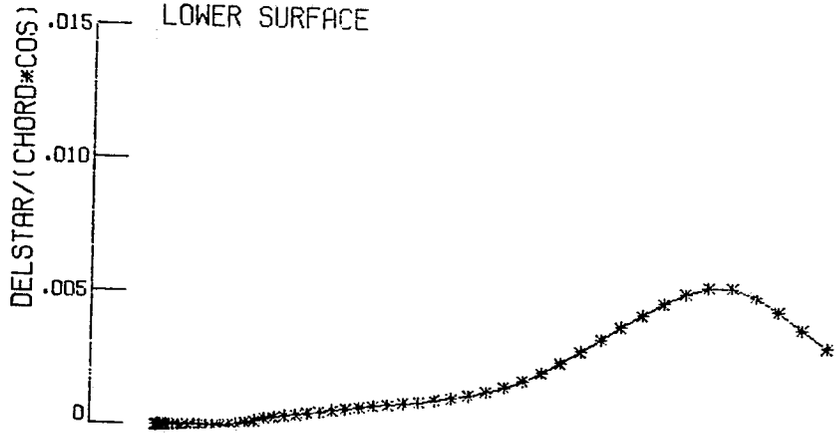

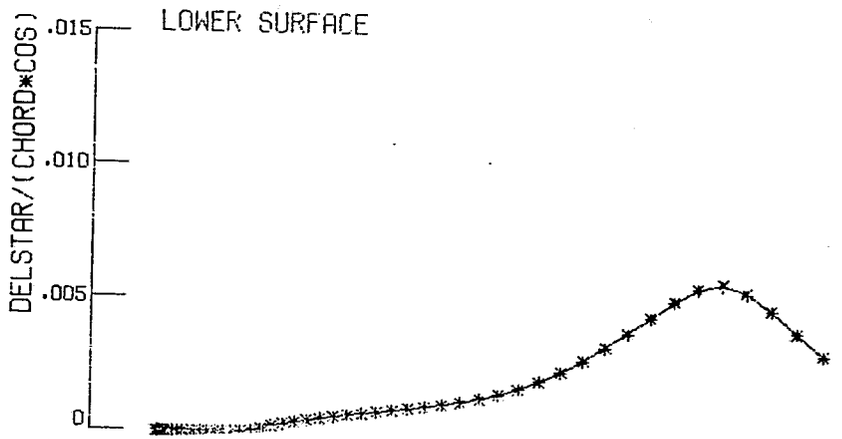

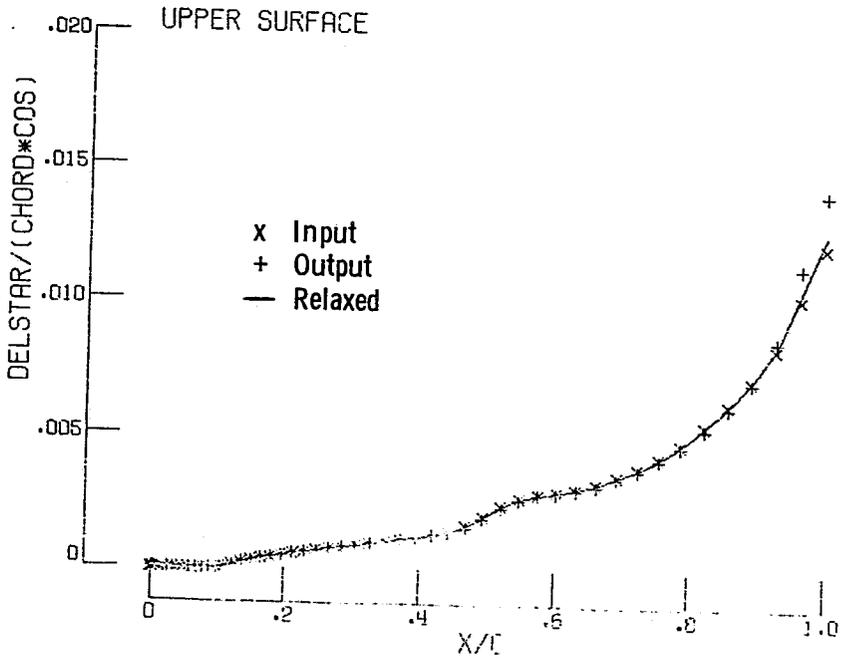

(c) 20 % semispan

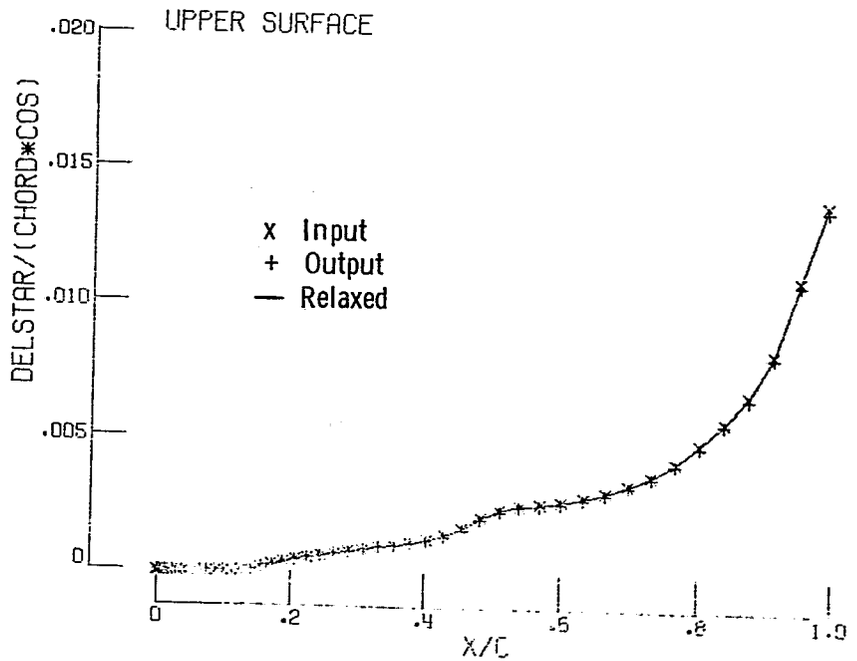

(d) 30 % semispan

Figure 4.- Continued.

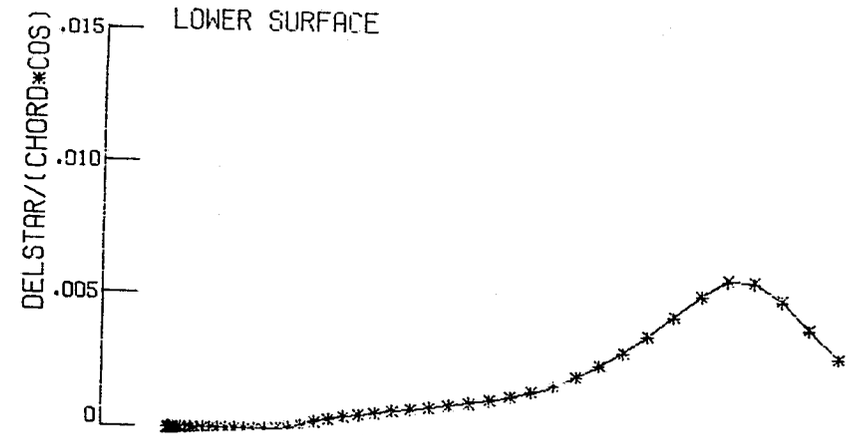

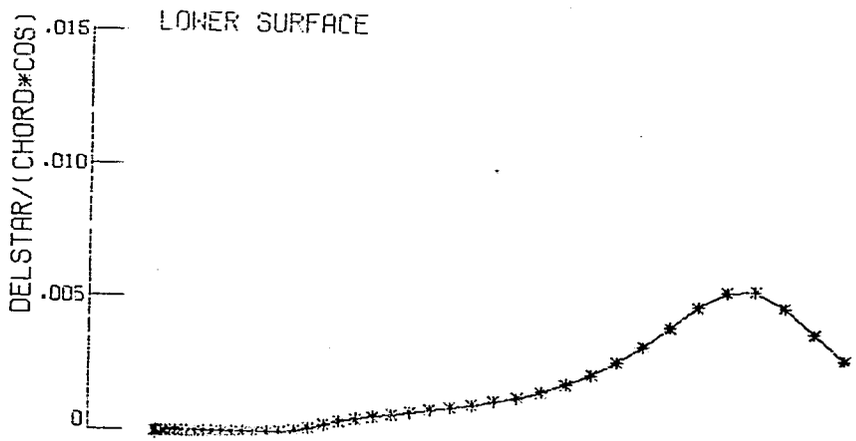

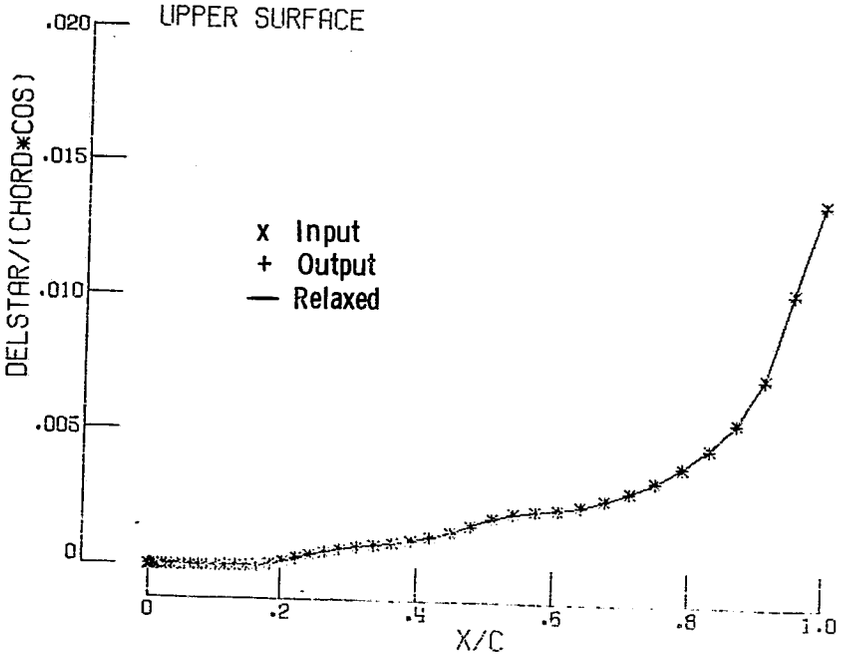

(e) 40 % semispan

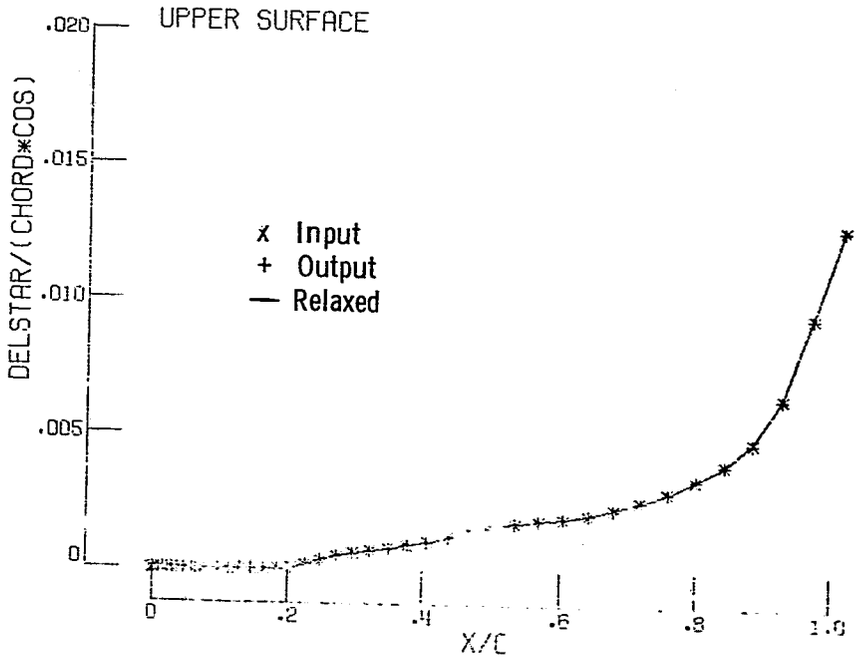

(f) 50 % semispan

Figure 4.- Continued.

ORIGINAL PAGE IS
OF POOR QUALITY

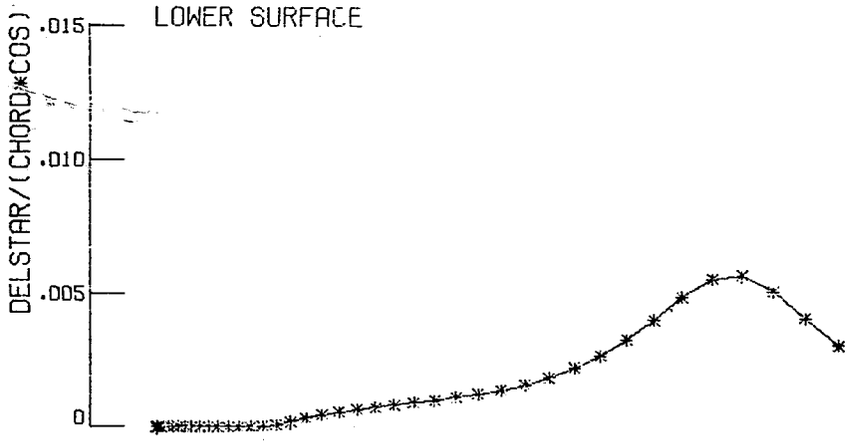

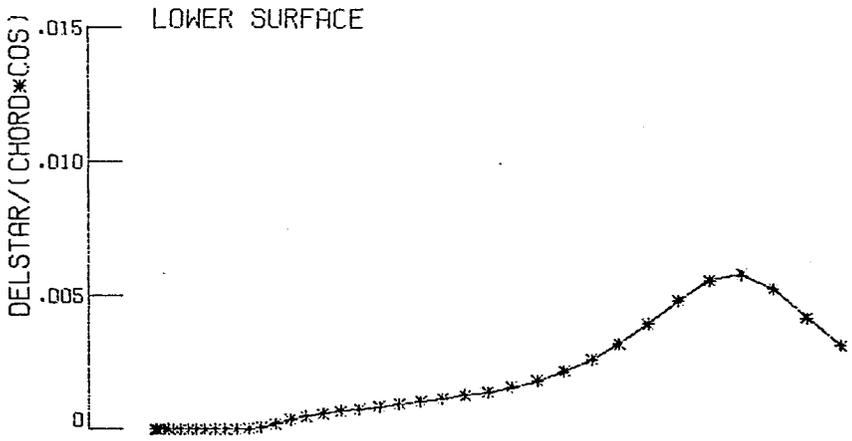

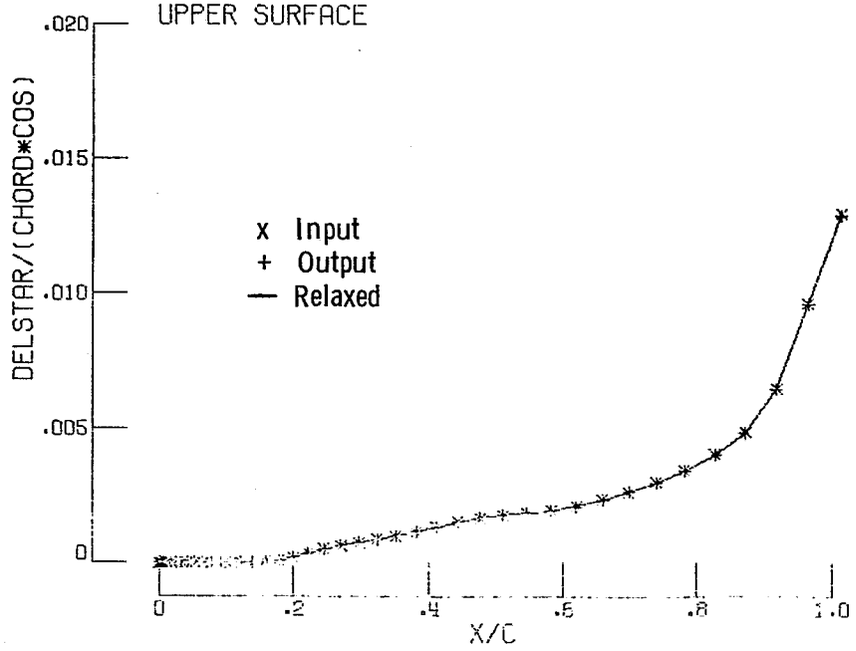

(g) 60 % semispan

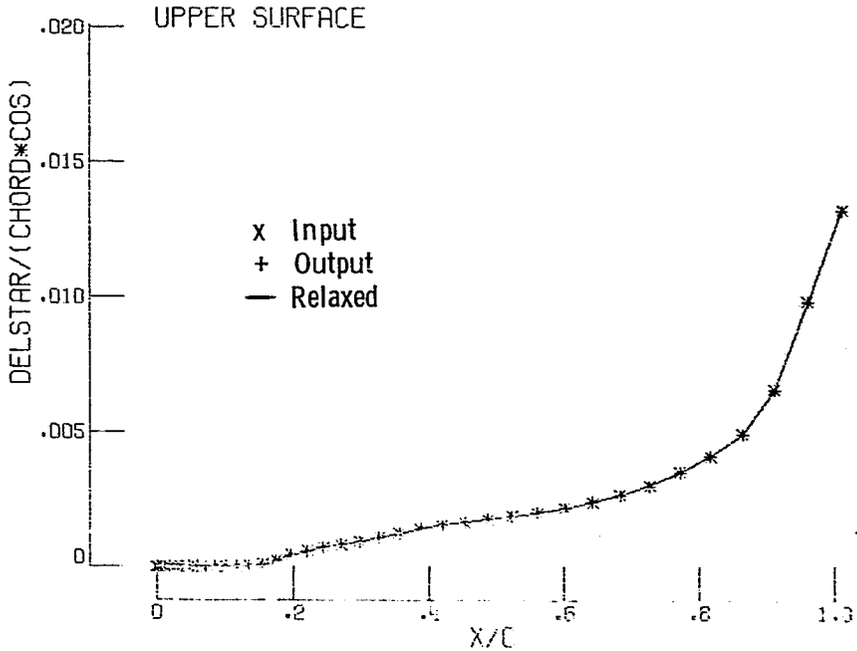

(h) 70 % semispan

Figure 4.- Continued.

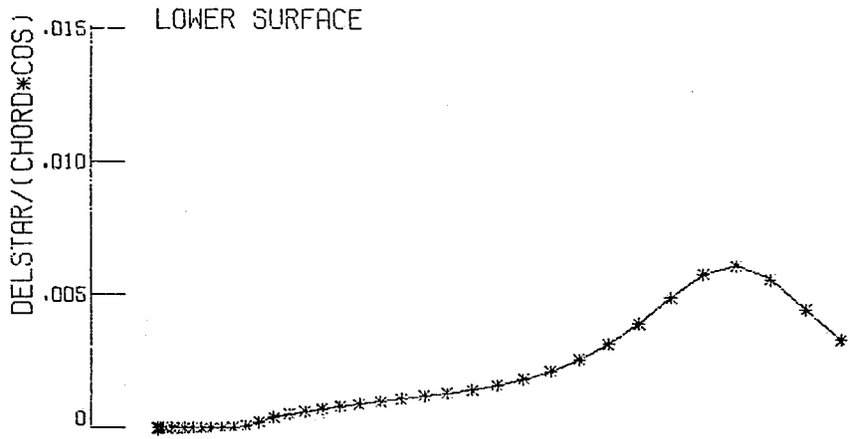

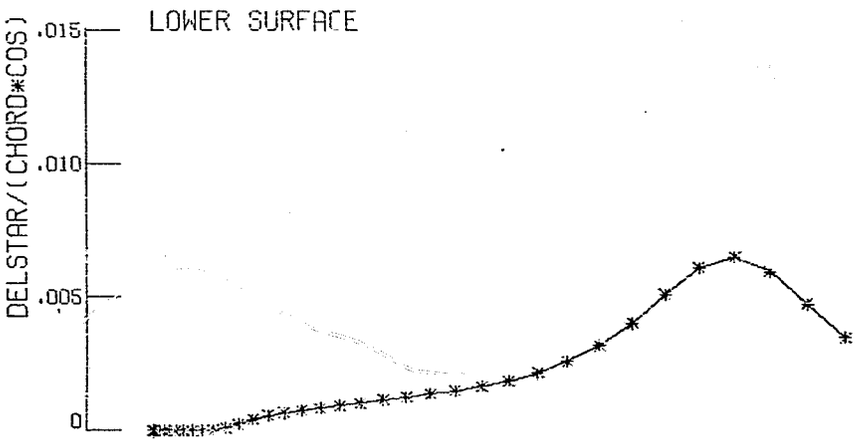

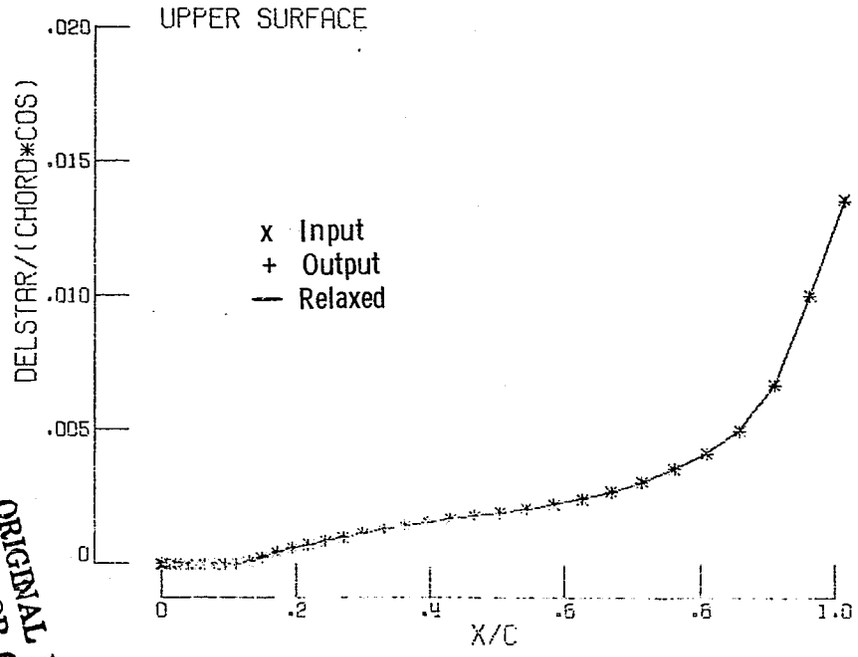

(i) 80 % semispan

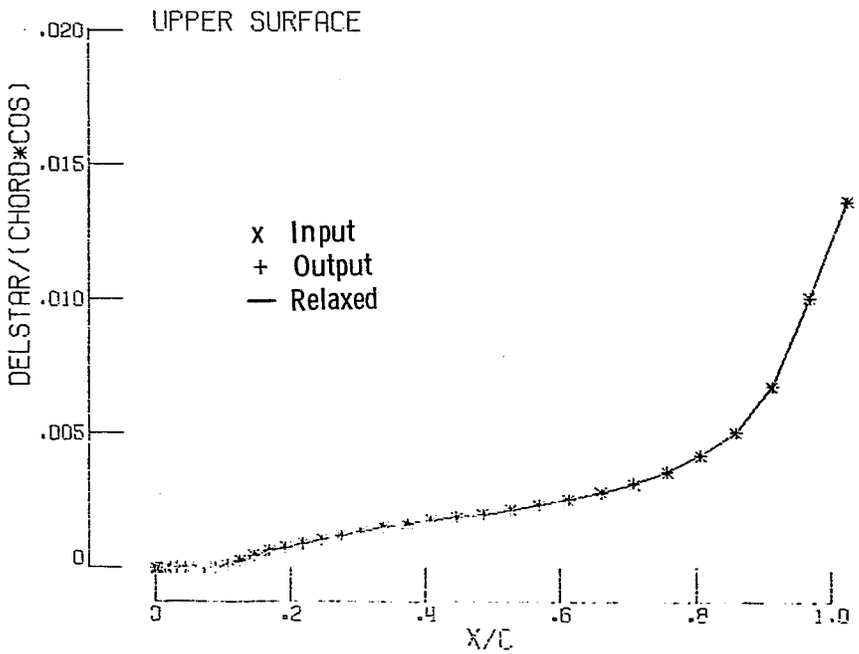

(j) 90 % semispan

ORIGINAL PAGE IS
OF POOR QUALITY

Figure 4.- Continued.

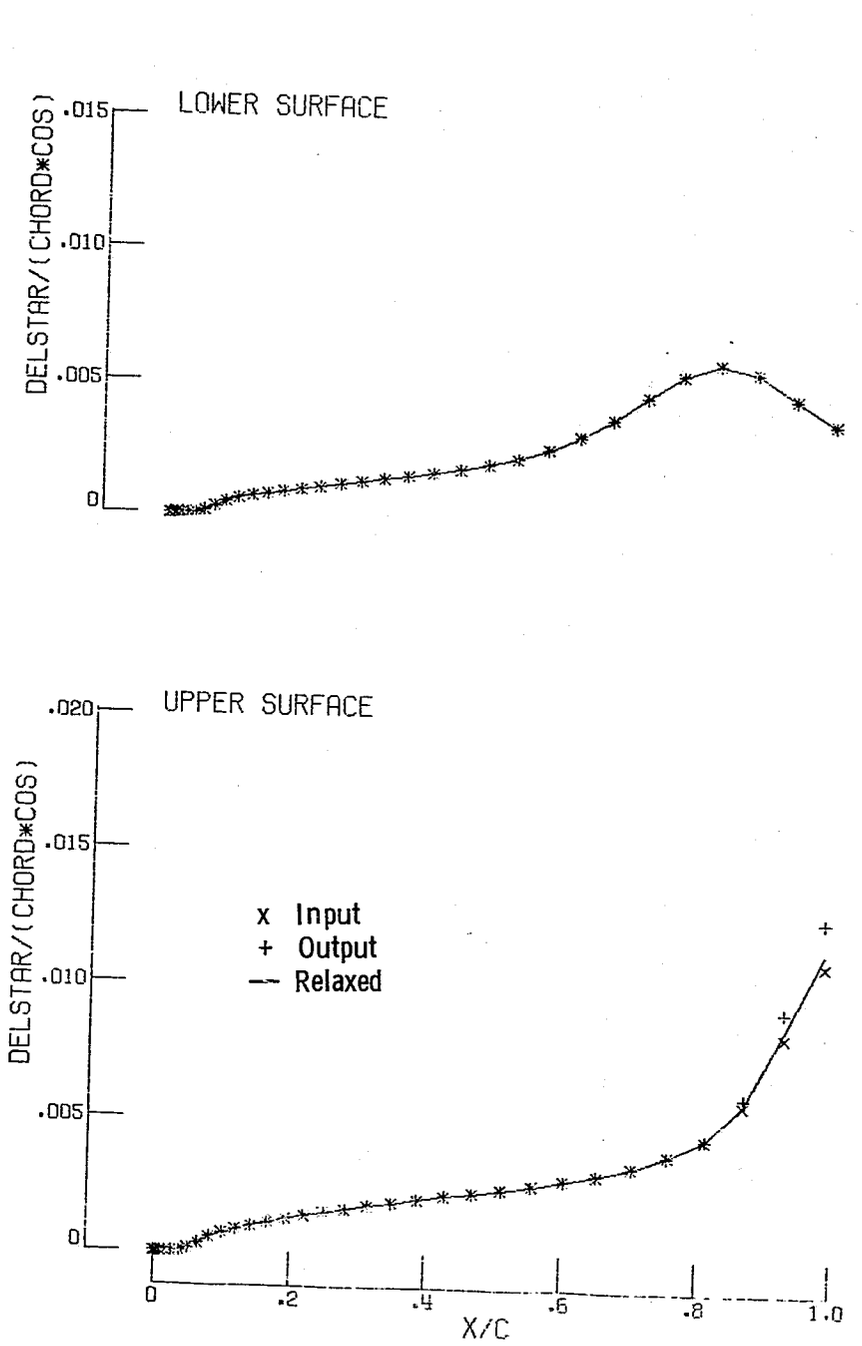

(k) 100 % semispan

Figure 4.- Concluded.

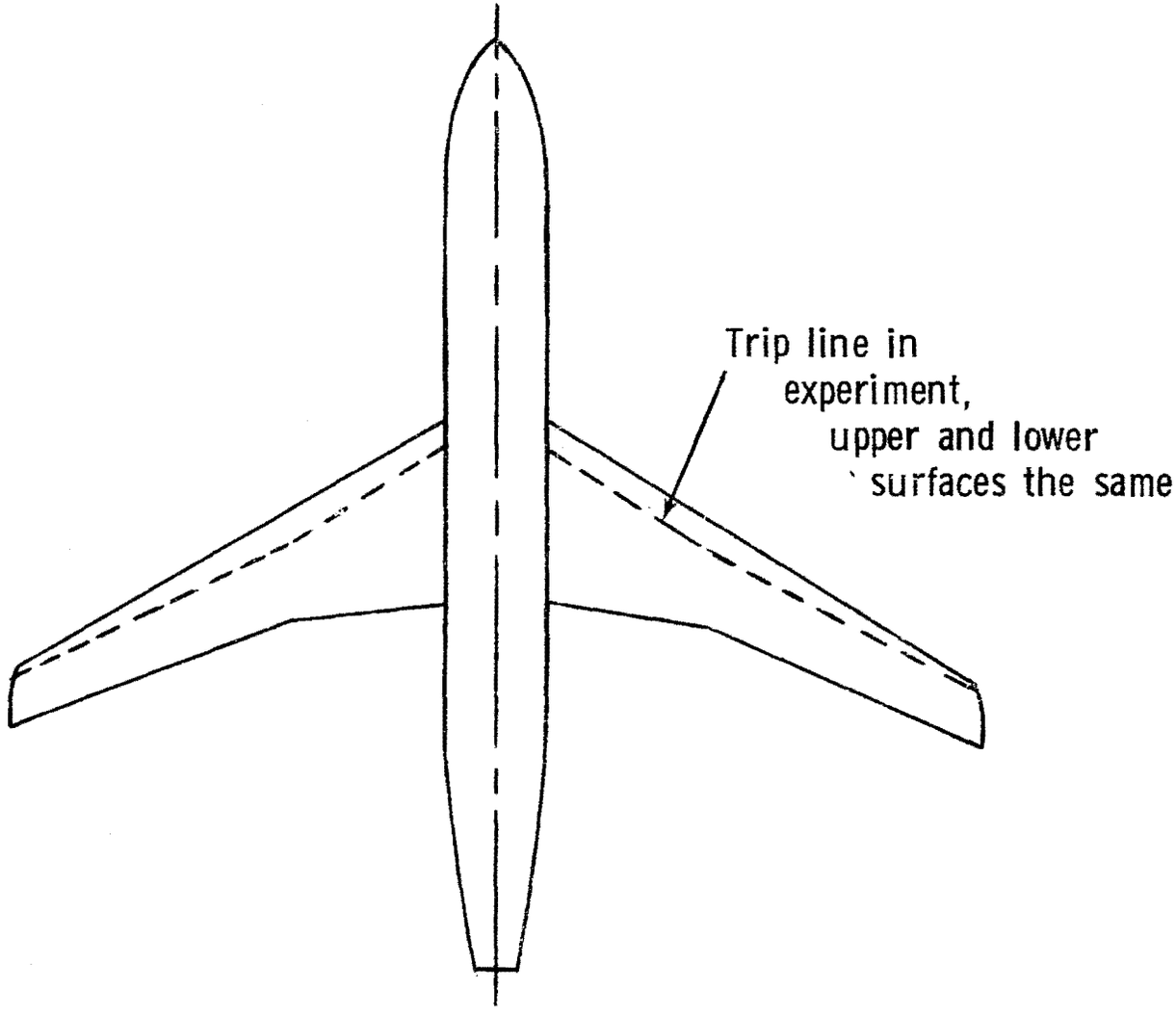

Figure 5.- Planform view of NASA supercritical wing low-mounted on a wide-body-type fuselage as tested by Bartlett; AR = 10.3, $\Lambda_{c/4} = 27^{0}$.

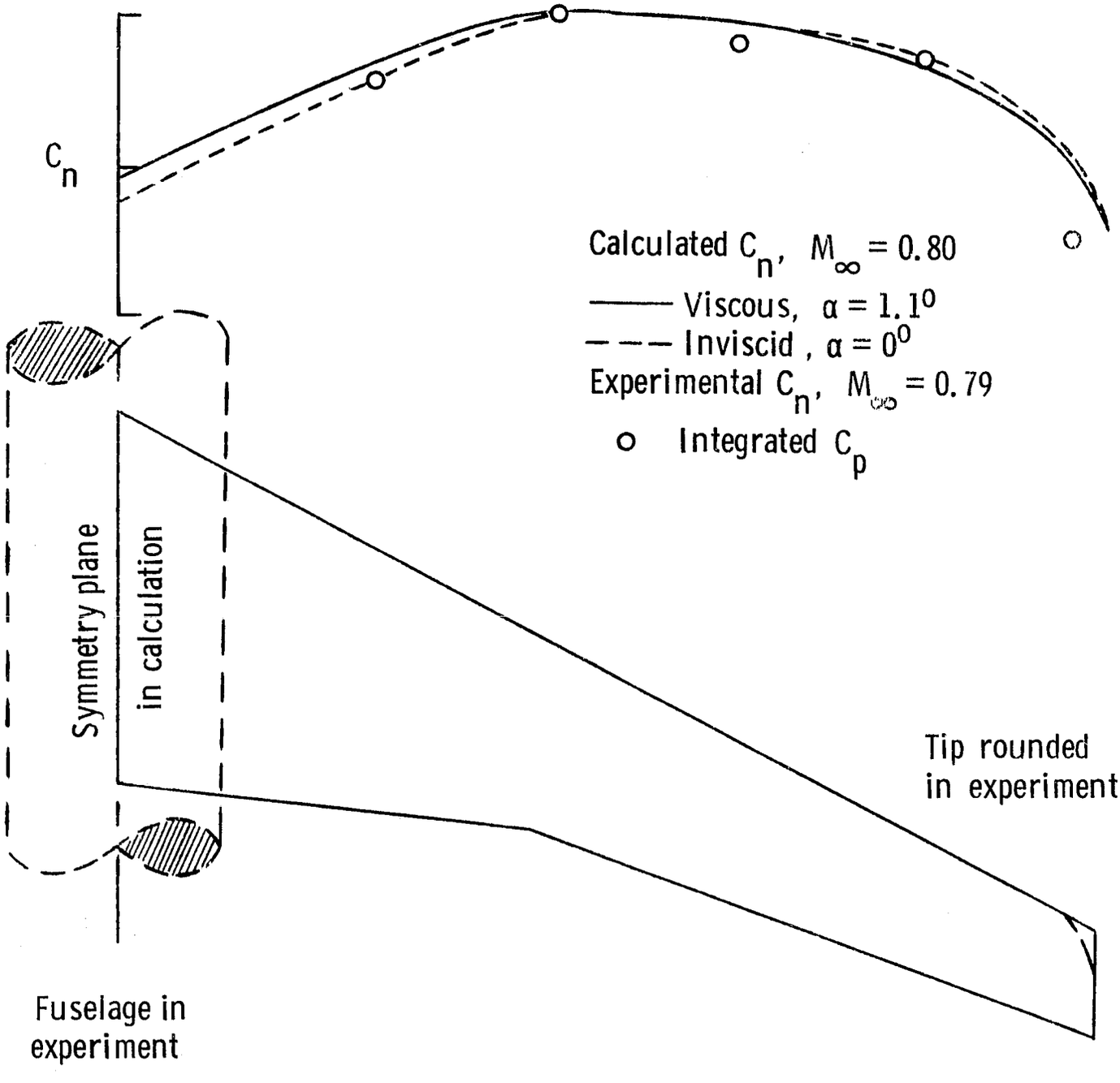

Figure 6.- Spanwise distribution of section normal force coefficient on NASA Supercritical wing showing manner of lift match.

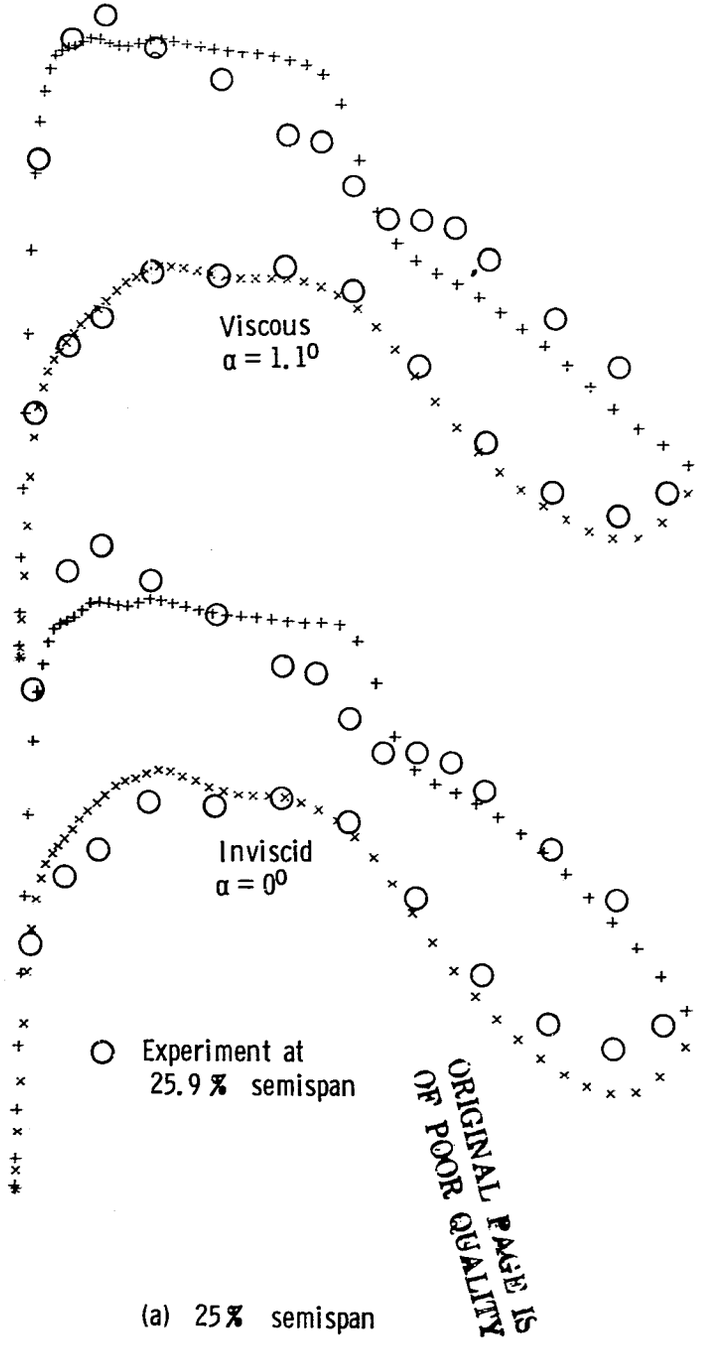

(a) 25% semispan

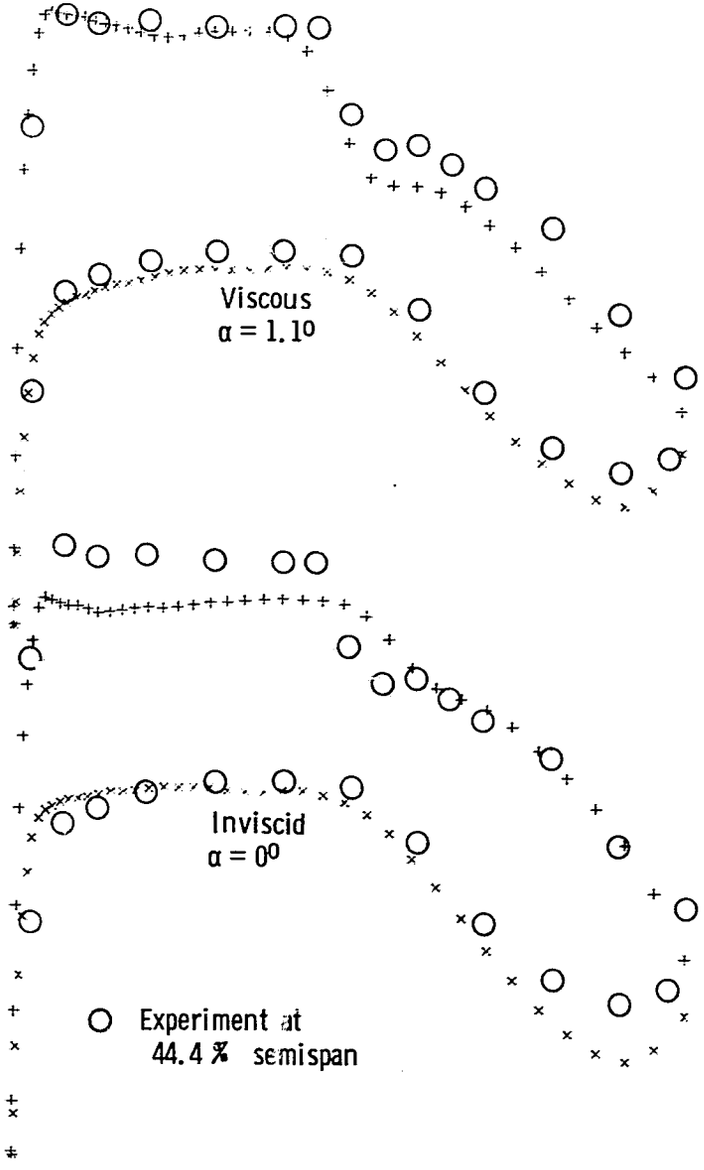

(b) 45% semispan

ORIGINAL PAGE IS
OF POOR QUALITY

Figure 7.- Comparison of present calculated (at $M_\infty = 0.80$) and Bartlett's experimental (at $M_\infty = 0.79$) chordwise distributions of surface pressure coefficients for a NASA Supercritical wing.

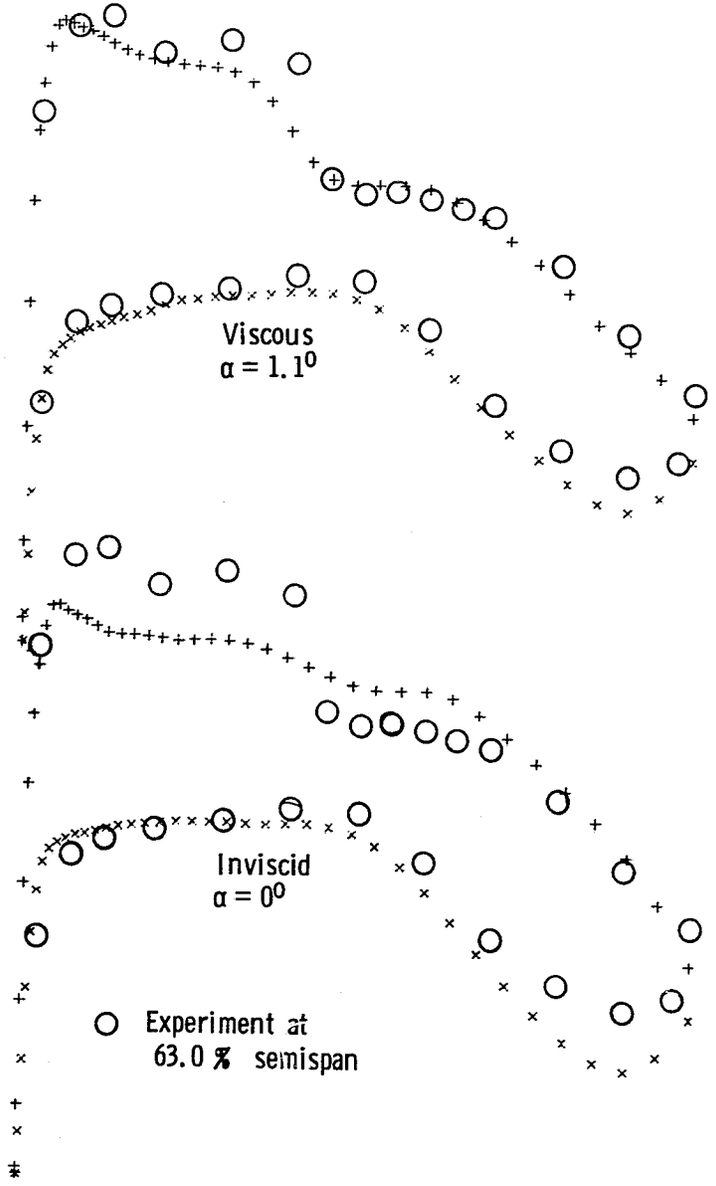

(c) 65 % semispan

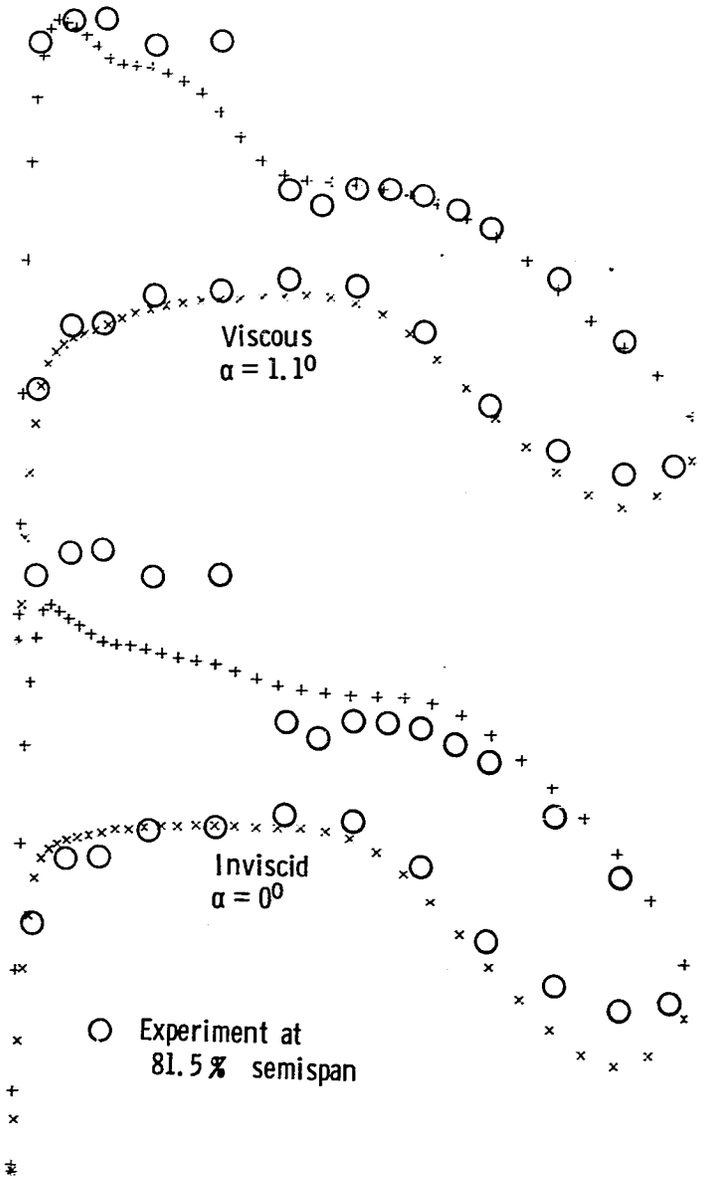

(d) 80 % semispan

Figure 7.- Continued.

(e) 95% semispan

Figure 7.- Concluded.

ORIGINAL PAGE IS
OF POOR QUALITY

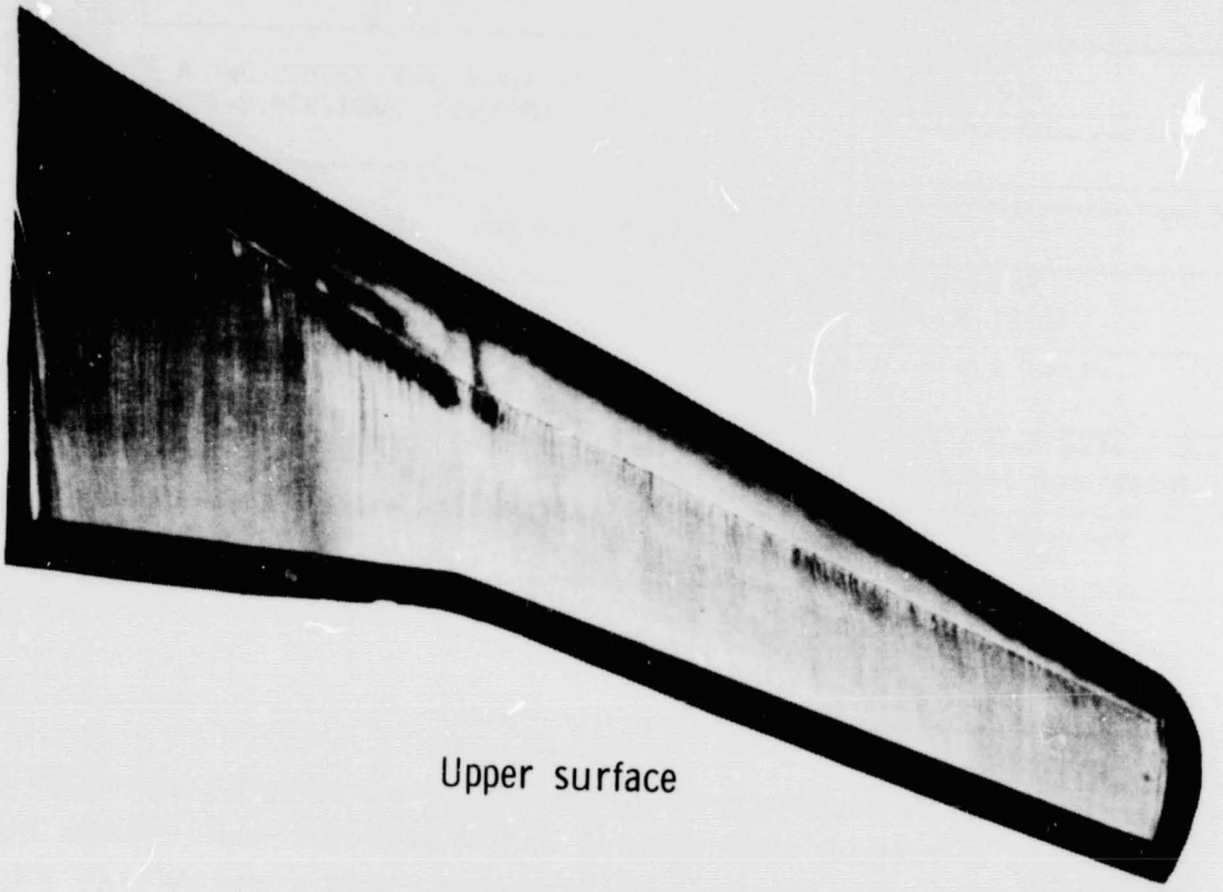

Upper surface

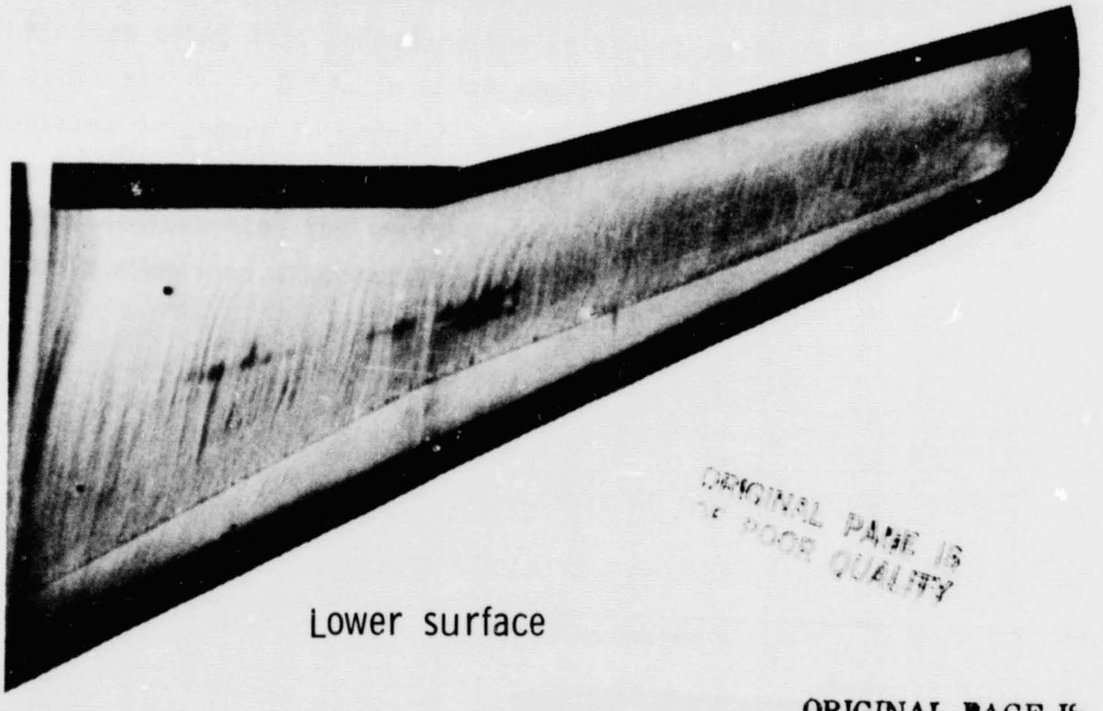

Lower surface

ORIGINAL PAGE IS
OF POOR QUALITY

Figure 8. - Oil flows on a NASA Supercritical wing.
$M_\infty = 0.79$, $C_L = 0.52$, $N_{Re} = 2.4 \times 10^6$ (based on MAC).